NATIONAL AERONAUTICS AND SPACE ADMINISTRATION

LUNAR SAMPLE ANALYSIS PROGRAM

"Neutron Activation Analysis for Rare Earths (Lanthanides and Yttrium) on Simulated Lunar Samples"

NGR 50-002-041

by Larry A. Haskin, Principal Investigator
Department of Chemistry
University of Wisconsin
Madison, Wis. 53706

Semiannual Progress Report, December 1968-May 1969
and Final Report

Prepared under Contract No. NAS 9-7975

For NASA Manned Spacecraft Center
Lunar Receiving Laboratory
Houston, Texas 77058

CR 101903

"Neutron Activation Analysis for Rare Earths (Lanthanides and Yttrium) on Simulated Lunar Samples"

Larry A. Haskin

ABSTRACT

Details and evaluation of a procedure are given for neutron activation analysis of the rare earths, based on separation of that element group from rocks and minerals and radioassay with a Ge-Li detector. Results for basaltic, intermediate, and rhyolitic rocks from the Stretishorn dike, Eastern Iceland, are presented and discussed in the light of recent geochemical studies for other elements in that body.

Further development of procedures for analysis of 40 elements by neutron activation, also based on element group separations and Ge-Li gamma-ray spectrometry, is discussed. Results obtained by this procedure are presented for 6 whole-rock chips and 4 separated phases from the Bruderheim meteorite.

Descriptors

General:

Neutron activation analysis
Rare-earth analysis
Analysis of Bruderheim chondrite
Multielement analysis
Analysis of igneous rocks

Specific:

Activation analysis for Halogens
Activation analysis for Alkali metals
Activation analysis for Alkaline earths
Activation analysis for Transition metals
Activation analysis for Rare Earths
Activation analysis with Ge-Li spectrometry
Separation of Pt-Pd metals
Stretishorn Icelandic Basalt and Rhyolite
Group separations

Contents

List of Tables

List of Figures

Summary

The development of a procedure for neutron activation analysis of the rare-earth elements La, Ce, Nd, Sm, Eu, Gd, Tb, Dy, Ho, Er, Yb, and Lu has been completed. The rare earths are separated as a group from the rock or mineral being analyzed, then counted a few hours, 3 days, 10 days, and 40 days after irradiation on a Ge-Li gamma spectrometer. A sample containing only 0.5 to 200 nanograms of the individual elements yielded values for 10 of the rare earths with statistical uncertainties of 10% or less.

This procedure was used to study the rare earth distribution in the basaltic, hybrid, and rhyolitic portions of the Stretishorn composite dike of eastern Iceland. The rare earths in the hybrid rocks correspond to a linear mixture of basalt and rhyolite parent, except for La, Ce, and possibly Tb. It is difficult to explain the rare-earth relative abundances in the rhyolite as having developed either by fractionation of basaltic magma or by assimilation of acid crustal material into basaltic magma.

The procedure for multielement analysis has been developed to the point that data for 6 whole-rock chips and 4 separated phases of the Bruderheim chondrite have been obtained. The 12 counting groups include the following elements: Ag, Br, Cl, Au, Ba, Pt, Mn, In, As, Cu, Pd, Sb, Se, Fe, Cr, Hf, Th(Pa), Sc, Ni, Co, Ga, Zn, Ca, Sr, Cs, K, Rb, and the 12 rare earths listed above. The precision of measurement depends both on the absolute amount of the element present and its amount relative to the other elements in the group. The data are still preliminary and subject to further correction, but are for the most part consistent with previous observations on meteorites and expectations based on the known chemical properties of the elements.

Neutron Activation Analysis for the Rare Earths

The reasons for developing a new procedure are discussed in detail in our previous report, where an outline of our method was presented. The following gives the details of our procedure and our evaluation of its accuracy, sensitivity, and applicability.

The method is based on separation of the rare-earths (RE) as a group from an activated rock or mineral, then gamma-ray spectrometry on that group with a high resolution Ge-Li detector. It is compatible with the relatively short neutron irradiations available at the University of Wisconsin nuclear reactor, which operates a few hours per day, three or four days per week.

Gordon et al (1968) and Cobb (1967) have described procedures for RE analysis based on Ge-Li gamma spectrometry of irradiated samples not subjected to chemical separation. In rocks of basic composition (USGS standards W-1 and BCR-1) Gordon et al. obtained values compatible with those obtained by various other methods for La, Ce, Sm, Eu, Tb, Tm, Yb, and Lu. Their analytical uncertainties ranged from $\pm$ 5% (Eu in BCR-1) to $\pm$ 26% (Tb in W-1), and averaged about $\pm$ 10%. Cobb reported values for W-1 for La, Sm, Eu, Dy, Yb, and Lu, with uncertainties ranging from $\pm$ 6% to $\pm$ 11%.

The sensitivity and accuracy of the above methods is strongly influenced by the radioactivity induced in elements other than the REE. These can readily be eliminated from the radioassay by chemical removal of the REE from the rest of the irradiated specimen. Tomura and coworkers (1968a,b) have developed such a procedure and have reported values for La, Ce, Nd, Sm, Eu, Gd, Tb, Dy, Tm, Tb, and Lu in W-1. Their values are compatible with others found in the literature, but estimates of analytical accuracy and sensitivity were not given. Their chemical separation is based on a hydroxide-fluoride precipitation cycle. Chemical yields were determined for the entire RE group by EDTA titration, which does not enable correction for fractionation within the RE group (i.e., selective loss of certain of the REE) resulting from the chemical processing, which can be quite serious.

In the development of our procedure we have benefitted from the above works and from experience with our older method (Haskin, et al., 1968).

Sample Preparation and Irradiation

Samples received as intact rocks are washed, scraped, or broken open and inside chips removed as appropriate for analysis. They are pulverized in mullite, diamonite, or hardened steel mortars as needed to keep possible contamination below detectible levels. The resulting powders, and samples received as powders are carefully mixed and 0.25gm portions are weighed and sealed into polyethylene tubes for irradiation alongside a RE solution monitor.

The standard monitor is a dilute solution of RE nitrates. The weight of each REE in 1 ml of the standard is given in Table 1. These weights are essentially those found in a gram of typical crustal material from the earth. Usually, not more than o.25gm of the standard monitor is irradiated.

To minimize effects of flux gradients, the standard monitor and samples are bound together with Scotch no. 549 pressure sensitive tape. To provide a first order correction for flux gradients, weighed, 5 cm strands of analytical reagent grade Fe wire are coiled and taped around those parts of the individual tubes that contain the samples and monitor. Final results are corrected for the ratios of specific activities of these wires, which usually are between 0.98 and 1.02. Significant improvement in analytical precision is obtained by this procedure.

Samples are irradiated from 0.5 to 5 hours at a flux of about 2×10^{13} n/cm^2/sec in the University of Wisconsin Nuclear Reactor, a pool type reactor with a Triga core.

Apparatus

The gamma-ray spectrometry is done with either of two Nuclear Diodes 20 cc coaxial GeLi detectors. The first, model LGC 2.5, is connected to a Canberra model 1408A preamplifier whose output is fed into a Canberra model 1417 spectroscopy amplifier. The resolution is 2.4 KeV for Co^{57} (122 KeV peak), 4.0 KeV for Cs^{137} (.662 KeV peak), and 6.7 KeV for Co^{60} (1.33 MeV peak). The second detector is a model LGC 2.2 XX, and is connected to a Tennelec model

Table 1. Concentrations of RE Standard Monitor and Carrier Solutions in Micrograms per Milliliter

	Standard Monitor	Carrier
Y	27.3	498
La	32.1	907
Ce	73.2	799
Pr	7.90	579
Nd	32.8	561
Sm	5.68	563
Eu	1.246	609
Gd	5.20	615
Tb	0.870	608
Dy	5.53	29.3
Ho	1.043	617
Er	3.42	702
Tm	1.017	876
Yb	3.06	912
Lu	0.944	908

TC 135 preamplifier which feeds to a Canberra model 1416 amplifier. Its resolution is 1.9 (Co^{57}), 2.3 (Cs^{133}), and 3.0 (Co^{60}) KeV. Each detector is enclosed in a 1.7 cm thick, approximately cubic lead shield, 50 cm on a side, to reduce background radiation at low energies due to U and Th series elements in the walls of our instrument room. The two detectors are located about 4 meters apart on opposite sides of a large iron shield that houses a NaI (Tl) scintillation crystal, so that samples being assayed in one do not register in the other.

The outputs of the amplifiers are routed into separate ADC's of a Nuclear Data model 2200, 4096 channel analyzer. The analyzer has digiplexing capability so that two separate spectra, one from each detector, can be routed into separate halves of its memory. When maximum resolution is required, the output from the detector of higher resolution can be expanded into the full memory. Adequate resolution for RE analysis is obtained by using only peaks below 1 MeV in energy and adjusting the amplifiers and ADC's to spread 1 MeV over 2,048 channels. 20 cc detectors are nearly as efficient for absorbing the low energy gamma rays of interest as are 30 cc and larger volume detectors of the same surface area.

The analyzer ADC's are usually completely stable during a day's time, but occasionally, from undetermined causes, they drift in energy from 1 to 5 channels. Whenever this occurs during a count, the resulting gamma peaks are correspondingly broadened and require special treatment as described in a later section. Perceptible broadening (about $^1/_3$ channel and greater) also occurs at high count rates, and to avoid this the ratio of elapsed counting time to analyzer live time must be kept below 1.5 for the first detector and 1.25 for the second.

Data are extracted from the analyzer memory with an IBM typewriter and a Houston Omnigraphic model 6550 point plotter. The analyzer is adjusted visually to plot and print only the desired portions of the spectra. The point plotter, when allowed to warm up for at least 5 minutes before use, produces graphs of sufficient accuracy to be used in determining peak baselines, as described in a later section. Data can also be extracted from the analyzer

memory onto paper tape for transfer to a computer. The spectra are sufficiently complex and the analytical method so new that we are still obliged to process the data manually.

Chemical Processing

Most of the work to be described later in this report was done on RE oxalate precipitates obtained by the chemical procedures described in our earlier work (Haskin et al., 1968) (stopping before ignition of the oxalate precipitate and further preparation for ion exchange). This procedure causes severe fractionation of the RE group, so that a titration of the combined group does not give a reliable chemical yield (Section on Chemical Yield Determination). Nearly all of this fractionation has been overcome by a new procedure developed as part of another project by Philip Helmke, and is now being used. The main steps in this new method are outlined below.

1) Dissolution of irradiated sample by fusion with Na_2O_2 in the presence of carrier. 2.0 ml of the RE nitrate carrier solution whose concentrations are given in Table 1 are evaporated into the zinconium crucibles prior to sample fusion.
2) Digestion of fusion cake with water and neutralization with HCl.
3) Precipitation of hydroxides with aqueous ammonia.
4) Dissolution of hydroxide precipitate with HCl and removal of silica by its precipitation with gelatin.
5) Precipitation of hydroxides with NaOH, dissolution in HCl, precipitation of oxalates.

Chemical yields of 95 to 99% are obtained with this procedure.

The oxalate precipitates are filtered onto circles of Whatman No. 50 filter paper, dried by rinsing with ethanol, then with ether, and mounted under polystyrene film (Saran Wrap) onto white cardboard for counting. Samples are ready for counting about 4 hours after the end of neutron irradiation.

Isotopes and Gamma Lines

All gamma-ray peaks observed from the activated REE in a sample of tholeiitic basalt (AD-80) at various times after

irradiation are listed in Tables 2-5. Portions of the spectra are shown in Figures 1-4. On the basis of the relative intensities of the various lines, mutual interferences among the REE, and minimization of the number of counts, four counting times per sample were selected. These times and the nuclides and gamma lines used from each are given in Table 6. Comments on interferences and peak selection are given below, element by element. When possible, two separate gamma lines are used for each nuclide and the nuclide is observed in more than one count set.

Lanthanum

The two dominant peaks from La^{140} give best precision in set II and good precision in set III, thus providing a measure of consistency between those count sets. In count set II, statistical uncertainties were less than $\pm$ 2% for basalts, in set III, 3-5%. There is sufficient overlap between the .3288 MeV peak, the Lu^{177} doublet at .3214 MeV, and the .3194 MeV Nd^{147} peak to invalidate the use of that line in set III whenever "whole peak" calculations are required, but when "half peak" calculations are used the effect is smaller than the statistical uncertainty (see section on calculations.) Among geologic samples, only those strongly depleted in La should violate this condition for set III, and the effect is always negligible in set II.

Cerium

Ce yields only one prominent line, .1454 MeV, from Ce^{141}. It can be used readily only in set IV, after the .1448 MeV line from Yb^{175} has decayed away. Counting of set IV at least 40 days after the end of neutron irradiation limits this interference to tenths of a percent for geologic samples. Statistical uncertainties for basalts are $\pm$ 3% or better. An analysis good to $\pm$ 10-15% can be obtained from the .293 MeV peak of Ce^{143} in set II, provided the Ce/Tb ratio in the sample is close to that of the standard monitor so that the Tb^{160} interference at .2985 MeV is the same for both.

TABLE 2. LIST OF GAMMA PEAKS OBSERVED IN AD-80 1/2 DAY AFTER ACTIVATION

Peak Channel	Peak Energy in MeV (Interpolated)	Assigned Transition (MeV)	Approximate Peak to Base Ratio
124 3/4	.0696	.0697 ^{153}Sm	1.2
135 1/4	.0753	.0754 ^{153}Sm	1.1
146	.0811	.0806 ^{166}Ho	1.1
161	.0893	.0895 ^{153}Sm	1.0
171	.0947	.0947 ^{165}Dy	3.6
186 5/8		.1032 ^{153}Sm	3.1
204	.1125	.1130 ^{177}Lu; .1138 ^{175}Yb	1.0
221 1/4		.1218 ^{152m}Eu	11.9
497 1/2	.2714	.2710 ^{152}Eu	1.1
513 1/2	.2800	.2798 ^{165}Dy	1.4
542 1/2	.2957	.2956 ^{171}Er	1.1
566	.3080	.3084 ^{171}Er	1.2
604	.3290	.3288 ^{140}La	1.2
632 1/2		.3444 ^{152m}Eu, ^{152g}Eu	2.9
664 1/2	.3619	.3617 ^{165}Dy	1.5
896	.4872	.4870 ^{140}La	1.3
1035	.5624	.5632 ^{152m}Eu	1.1
1160	.6300		1.1
1166 1/2		.6335 ^{165}Dy	1.1
1290	.7004	.700 ^{152}Eu	1.1

TABLE 2 (CONTINUED)

1317 1/2	.7154	.700	^{165}Dy	1.1
1502 1/2	.8158	.8158	^{140}La	1.2
1550		.8416	^{152m}Eu	7.3
1773 1/2		.9633	^{152m}Eu	7.2
2420	1.3154	1.3150	^{152m}Eu	1.9
2552 1/2	1.3876	1.3893	^{152m}Eu	2.0
2688	1.461	1.460	^{40}K	2
2936		1.5966	^{140}La	10

TABLE 3. LIST OF GAMMA PEAKS OBSERVED IN AD-80 $3\frac{1}{2}$ DAYS AFTER ACTIVATION

Peak Channel	Peak Energy in MeV (Interpolated)	Assigned Transition (MeV)	Approximate Peak to Base Ratio
16 1/2	.0634	.0631 ^{169}Yb	1.2
28 3/8		.0697 ^{153}Sm	2.0
39 3/4	.0755	.0754 ^{153}Sm	1.2
49 5/8	.0810	.0806 ^{166}Ho	1.3
80 5/8	.0976	.0974 ^{153}Sm, ^{153}Gd	1.5
91 1/8		.1032 ^{153}Sm	6.8
104	.1101	.1098 ^{169}Yb	1.2
110 1/4	.1134	.1138 ^{177}Lu, ^{175}Yb	1.8
125 7/8		.1218 ^{152m}Eu, ^{152g}Eu	2.8
143	.1308	.1305 ^{169}Yb	1.2
169 3/8	.1450	.1454 ^{141}Ce; .1448 ^{175}Yb	1.4
199	.1609		1.0
212 1/2	.1681		1.1
221 1/4	.1728	.1729 ^{153}Sm	1.2
229 1/2	.1773	.1772 ^{169}Yb	1.1
267 5/8	.1977	.1980 ^{169}Yb; .1970 ^{160}Tb	1.3
287 1/2		.2084 ^{177}Lu	1.9
300 1/2	.2153	.2153 ^{160}Tb	1.1
353	.2434		1.1
396 1/2	.2668		1.1

TABLE 3 (CONTINUED)

426	.2826	.2826	^{175}Yb	1.7
445 3/4	.2932	.293	^{143}Ce	1.2
455 1/2	.2984	.2985	^{160}Tb	1.1
472 1/2	.3075	.3078	^{169}Yb	1.1
512 1/4		.3288	^{140}La	3.3
541 1/4	.3446	.3444	$^{152m}Eu, ^{152g}Eu$	1.6
576	.3630			1.0
615 1/2	.3840			1.0
638 1/2	.3965	.3961	^{175}Yb	2.1
706 1/2	.4328	.4325	^{140}La	1.3
807 3/4		.4870	^{140}La	4.1
889 1/2	.5309	.5312	^{147}Nd	1.1
970 1/2	.5742	.5746	^{140}La	1.1
1301 1/2	.7513	.7518	^{140}La	1.3
1422		.8158	^{140}La	2.5
1470 1/2	.8411	.8416	^{152m}Eu	1.7
1519 1/2	.8674	.8678	^{140}La; .869 ^{152g}Eu	1.3
1559	.8886	.8893	^{46}Sc	1.2
1626	.9245	.9252	^{140}La	1.4
1698	.9630	.9633	$^{152m}Eu, ^{152g}Eu$	1.7
1925	1.0847	1.0856	^{140}La	1.0
1992 1/2	1.1209	1.1205	^{46}Sc	1.3

TABLE 3 (CONTINUED)

2352	1.3136	1.315 ^{152m}Eu	1.1
2527	1.4074	1.408 ^{152g}Eu	1.1
2623	1.4588	1.460 ^{40}K	1
2697	1.4985	1.500 ^{140}La	1
2880		1.5966 ^{140}La	14
3643	2.0056		2
3782	2.0801		1

TABLE 4. LIST OF GAMMA PEAKS OBSERVED IN AD-80 11 DAYS AFTER IRRADIATION

Peak Channel	Peak Energy in MeV (Interpolated)	Assigned Transition (MeV)	Approximate Peak to Base Ratio
108 3/8	.0631	.0631 ^{169}Yb	1.3
120 5/8		.0697 ^{153}Sm	1.7
131 1/8	.0754	.0754 ^{153}Sm	1.2
152 3/4	.0870	.0868 ^{160}Tb	1.3
160 5/8	.0912	.0910 ^{147}Nd	1.3
172 1/2	.0976	.0974 ^{153}Sm, ^{153}Gd	1.2
182 7/8		.1032 ^{153}Sm	5.8
195 1/2	.1100	.1098 ^{169}Yb	1.5
201 5/8	.1133	.1130 ^{177}Lu	2.1
217 1/2		.1218 ^{152g}Eu	4.4
233 3/4	.1306	.1305 ^{169}Yb	1.6
246 1/2	.1375	.1376 ^{175}Yb	1.1
261	.1453	.1454 ^{141}Ce; .1448 ^{175}Yb	3.8
288 1/2	.1602		1.1
312	.1730	.1729 ^{153}Sm	1.1
319 3/4	.1772	.1772 ^{169}Yb	2.0
357 7/8	.1978	.1980 ^{169}Yb; .1970 ^{160}Tb	2.9
377 3/8		.2084 ^{177}Lu	4.1
391 3/8	.2159	.2156 ^{160}Tb	1.3
444 1/2	.2448	.2447 ^{152g}Eu	2.0

TABLE 4 (CONTINUED)

475	.2613	.2610	^{169}Yb	1.0
514 5/8	.2827	.2826	^{175}Yb	2.7
544	.2986	.2985	^{160}Tb	2.4
560 7/8	.3078	.3077	^{169}Yb	1.5
584 1/2	.3206	.3214	^{177}Lu; .3194 ^{147}Nd	1.1
599 3/4		.3288	^{140}La	2.0
628 5/8	.3446	.3444	^{152c}Eu	4.0
724 5/8	.3964	.3961	^{175}Yb	4.0
751 1/2	.4108	.4112	^{152c}Eu	1.2
789 5/8	.4314	.4325	^{140}La	1.2
812 1/2	.4438	.4442	^{152g}Eu	1.3
892 1/2		.4870	^{140}La	2.7
973	.5304	.5310	^{147}Nd	1.3
1430	.7785	.779	^{152g}Eu	1.5
1498	.8154	.8158	^{140}La	1.5
1594 1/2	.8679	.869	^{152g}Eu; .8678 ^{140}La	1.3
1616 1/2	.8798	.8793	^{160}Tb	1.5
1634		.8893	^{46}Sc	2.3
1700 1/2	.9254	.9252	^{140}La	1.1
1772	.9648	.965	^{152g}Eu	2.3
1997 1/2	1.087	1.087	^{152g}Eu	1.7
2060 1/2	1.1215	1.1205	^{46}Sc	3.7
2167	1.1793	1.1777	^{160}Tb	1.5

TABLE 4 (CONTINUED)

2541 1/2	1.2741	1.2723	^{160}Tb	1.5
2587	1.4073	1.408	^{152g}Eu	2.2
2683 1/2	1.4598	1.462	^{40}K	1
2935 1/2		1.5966	^{140}La	6

TABLE 5. LIST OF GAMMA PEAKS OBSERVED IN AD-80 36 DAYS AFTER ACTIVATION

Peak Channel	Peak Energy in MeV (Interpolated)	Assigned Transition (MeV)	Approximate Peak to Base Ratio
108 5/8	.0629	.0631 ^{169}Yb	1.4
152 5/8	.0866	.0866 ^{160}Tb	2.2
161	.0912	.0910 ^{147}Nd	1.3
172 5/8	.0974	.0974 ^{153}Gd	1.3
183 3/8	.1032	.1032 ^{153}Gd	1.3
195 1/2	.1098	.1098 ^{169}Yb	1.7
201 1/2	.1130	.1130 ^{177}Lu	1.1
217 7/8		.1218 ^{152g}Eu	7.4
234 1/8	.1306	.1305 ^{160}Yb	1.8
261 5/8		.1454 ^{141}Ce	4.9
290 5/8	.1611		1.1
320 1/2	.1773	.1772 ^{169}Yb	2.5
358 1/2	.1978	.1980 ^{169}Yb; .1970 ^{160}Tb	3.8
378	.2083	.2084 ^{177}Lu	1.8
391 1/2	.2156	.2156 ^{160}Tb	1.6
445 3/8		.2447 ^{152g}Eu	3.3
477	.2618	.2610 ^{169}Yb	1.0
514	.2818	.2826 ^{175}Yb	1.1
544 7/8	.2986	.2985 ^{160}Yb	4.0
562 1/2	.3081	.3077 ^{169}Yb	1.5

TABLE 5 (CONTINUED)

617	.3376	.3371 ^{160}Tb	1.1
629 5/8		.3444 ^{152g}Eu	7.1
672	.3673	.367 ^{152g}Eu	1.3
718	.3922	.3924 ^{160}Tb	1.2
725	.3959	.3961 ^{175}Tb	1.1
753 1/2	.4113	.4112 ^{152g}Eu	1.6
814 3/8		.4442 ^{152g}Eu	1.7
1332	.7239	.724 ^{154}Eu	1.2
1434	.7791	.779 ^{152g}Eu	2.3
1596 1/2	.8670	.869 ^{152g}Eu	1.5
1620	.8797	.8793 ^{160}Tb; .876 ^{154}Eu	1.6
1637 3/4		.8893 ^{46}Sc	3.1
1776	.9640	.965 ^{152g}Eu; .9664 ^{160}Tb	
		.9628 ^{160}Tb	3.8
1851	1.0046	1.007 ^{154}Eu; 1.000 ^{154}Eu;	
		1.006 ^{152g}Eu; 1.003 ^{160}Tb	2
2001 1/2	1.0860	1.087 ^{152g}Eu	3
2053	1.1139	1.113 ^{152g}Eu; 1.115 ^{160}Tb	4
2065 1/4		1.1205 ^{46}Sc	8
2170 1/4	1.1775	1.1777 ^{160}Tb	2
2211 1/2	1.1999	1.200 ^{160}Tb	1

TABLE 5 (CONTINUED)

2232 1/2	1.2113	1.213 ^{152g}Eu	1
2346 1/2	1.2732	1.2723 ^{160}Tb	3
2388	1.2958	1.298 ^{152g}Eu	2
2417	1.3115	1.312 ^{160}Tb	2
2594 1/2		1.408 ^{152g}Eu	15
2690	1.460	1.462 ^{40}K	4
2814	1.527	1.525 ^{152g}Eu	2
2932	1.591	1.597 ^{140}La	2

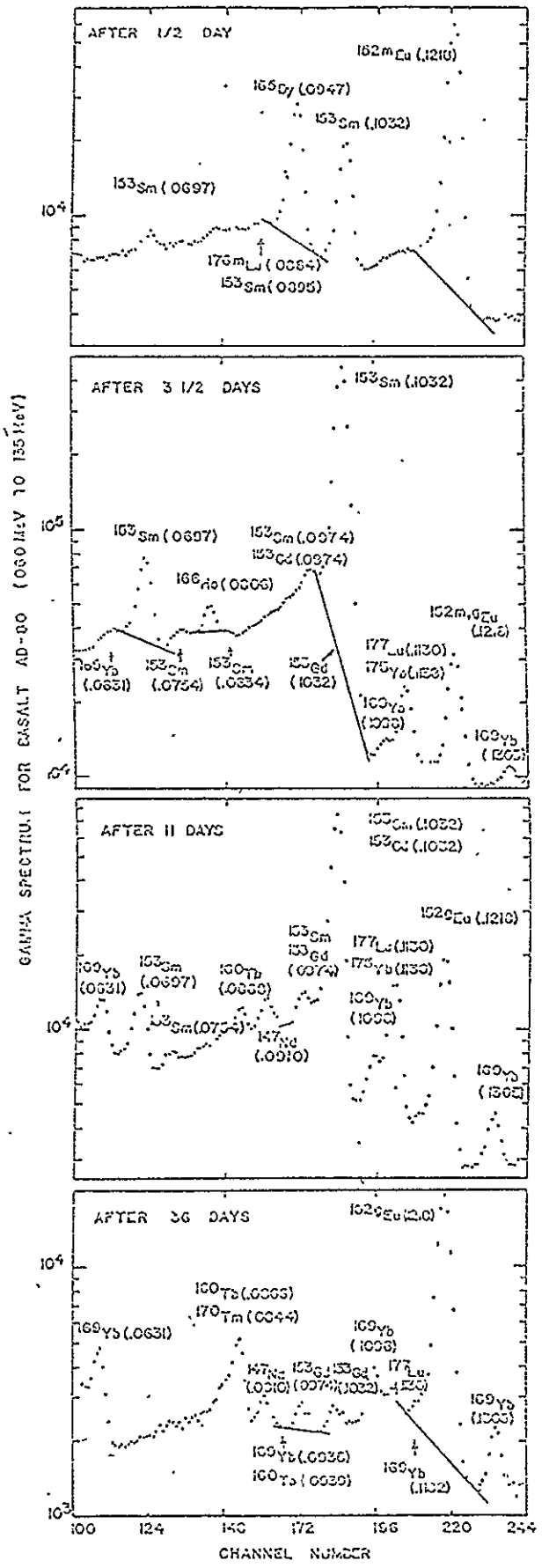

Figure 1. Gamma-Ray Spectra for Basalt AD-80; 0.60 to .135 MeV

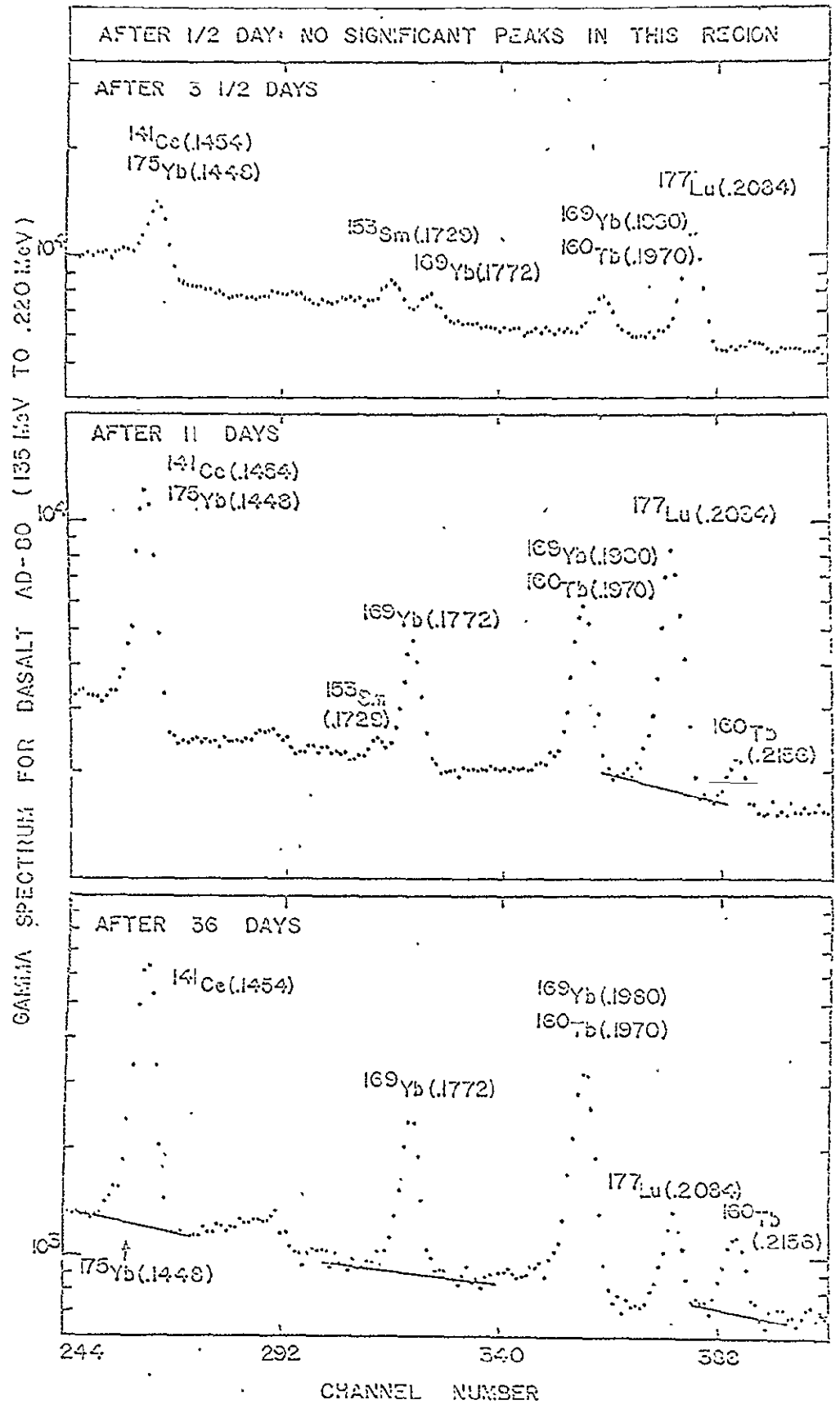

Figure 2. Gamma-Ray Spectra for Basalt AD-80; .135 to .220 MeV

Figure 3. Gamma-Ray Spectra for Basalt AD-80; Above .220 MeV

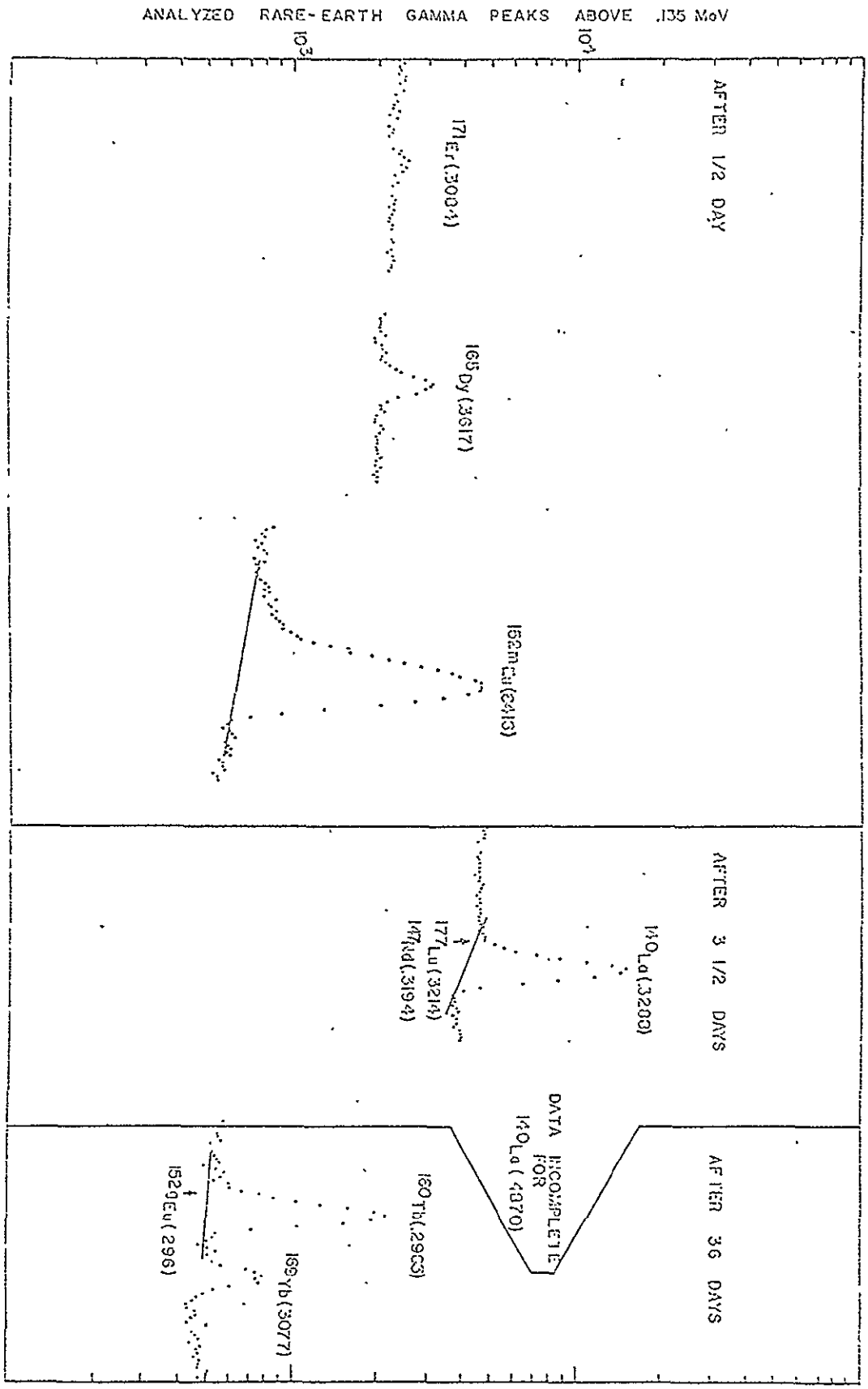

Figure 4. Gamma-Ray Spectra for Basalt AD-80; Above .220 MeV

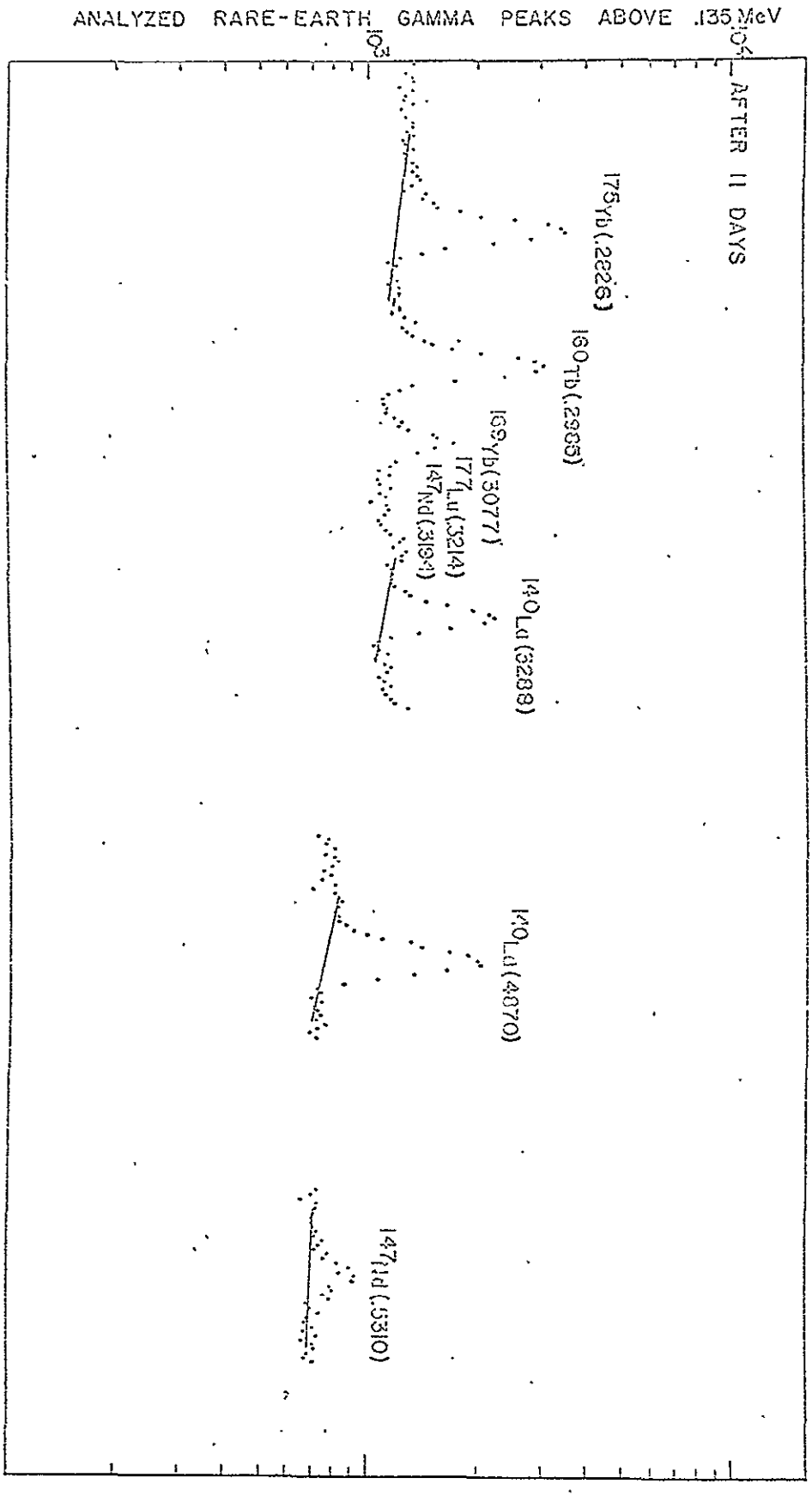

Praseodymium

This is the only naturally-occurring lanthanide for which no peak appears in any count set.

Neodymium

Nd^{147} yields two peaks best observed in count set III. Unfortunately, the interference from other nuclides is so severe in the energy region .085-.100 MeV that the stronger Nd^{147} peak at .0910 MeV cannot be used. The peak at .5310 MeV is isolated, but is so weak that statistical uncertainties of the order of $\pm$ 20% usually result.

Samarium

Peaks from Sm^{153} are easily observed in count sets I-III and dominate the spectrum at low energies in set II. Peaks at .1032 and .0697 MeV give statistical uncertainties of about 1.5 and 4%, respectively, in basalts. There are, unfortunately, somany competing peaks in the energy region .085-.100 MeV that some uncertainty arises in drawing the baseline for the .1032 MeV peak. This difficulty is usually overridden by the dominance of that peak.

In cases where the Sm/Yb ratio in the standard differs markedly from that of the sample, the contribution from the .0631 MeV peak of Yb^{169} can affect the position of the baseline for the Sm^{153} .0697 peak, and the results from the .1032 MeV peak are superior, especially if whole peak calculations are required.

Sm peaks can also be analyzed in the first and third count sets to provide consistency checks. A small correction is required in the third count set for contributions from Gd^{153}, which decays to the same excited states of Eu^{153} as does Sm^{153}.

Europium

Major contributions to all four count set spectra are present from Eu^{152} and Eu^{152m}. Peaks from Eu^{152m} at .1218 and .3444 MeV have been chosen for analysis in set I, then the .1218 MeV peak of Eu^{152} is analyzed from sets III and IV for consistency checks. This cannot be done conveniently in set II because of the mixture of 9.3 hour and 12.4 year activities.

There is a small interference from the .1182 MeV line of Yb^{169}, but this can be neglected in "half-peak" calculations except in rare (not yet encountered) cases where visible peaks adjacent to the .1218 MeV Eu^{152} peak are of the same order of magnitude as the .1218 MeV peak. It must be checked in "whole peak" calculations, but has proved to be insignificant for all analyses made so far.

Statistical uncertainties for Eu from basalts are normally less than $\pm$ 2%.

Gadolinium

Only the peak at .0974 MeV from Gd^{153} can be used for Gd analysis, and it gives marginal results. It is best used in count set IV, and care must be taken to minimize effects of a hidden Yb^{169} peak at .0936 MeV which raises the apparently decent valley between the Gd^{153} .0974 MeV peak and the adjacent .0910 MeV Nd^{147} peak. This can cause errors of 15-25% in integrating under the Gd^{153} .0974 MeV peak, and corresponding errors in analysis depending on how different the Gd/Yb ratio in the sample is from that of the standard monitor. The Yb^{169} interference is removed by decay about 6 months after irradiation of the sample, but an additional long count would be required merely to improve slightly the Gd values, and would also delay chemical yield determinations. To minimize the effects of the interference, only the top 3 channels in the Gd^{153} .0974 MeV peak are used, provided that peak broadening due to analyzer drift has not occurred. This practice reduces the relative importance of the baseline, which is the major source of systematic error for this element.

Statistical uncertainties for Gd are at least $\pm$ 10% for basalts.

Terbium

Peaks from Tb^{160} first appear in count set II and are a major feature of the spectrum in set IV. Remarkably, of the several peaks that appear, only the one at .2985 MeV is both strong and isolated enough to be useful for precise analysis. Even this peak suffers from a small interference from Eu^{152} at 0.296 MeV, which introduces a systematic error into peak area calculations of about

the same size as the statistical uncertainty (1-2%). Since the baseline is otherwise free from interference and there are reference lines from Eu^{152} in the spectrum, the appropriate correction can readily be made. Because of the variability of relative Eu abundances in nature, it is not feasible always to use a standard monitor that has about the same Tb/Eu ratio as the sample.

Dysprosium

Of the several Dy^{165} peaks that appear in the first count set, those of .0947, .2798, and .3617 MeV are most suitable for analysis. The .3617 MeV peak is isolated, but small relative to the Compton background underneath, and in basalts has a statistical uncertainty of $\pm$ 8-10%. The more intense .0947 MeV peak has a statistical uncertainty of only about $\pm$ 2%, but is subject to systematic negative errors of peak integration because its baseline is affected by .0884 MeV Lu^{176m} and .0895 MeV Sm^{153} peaks. The magnitude of this error decreases with increasing intensity of the Dy^{165} peaks relative to the underlying Compton background. The ultimate error thus depends in part on the Dy/Sm and Dy/Lu ratios in the samples and the standards, and in part on the extent of decay of the 2.35 hour Dy^{165} during the first count set, which usually spans 2 to 3 half-lives for that element.

Results from the Dy^{165} .0947 and .3617 MeV peaks often fail to agree within their statistical uncertainties. Calculations based on the third most intense Dy^{165} peak (.2798 MeV) agree better with results from the .3617 MeV peak than with those from the .0947 MeV peak. Thus, whenever the statistical uncertainty for the .3617 peak is $\pm$ 10% or less, the resulting value is taken as the correct one. When the uncertainty exceeds 10%, the values from the .3617 and .0947 MeV peaks are averaged. The .2798 MeV peak is sufficiently intense in many samples to be useful when counting is done soon enough after irradiation.

Holmium

Ho^{166} yields a peak at .0806 MeV that can be used for analysis in count set II. While the intensity is adequate, so many small interference peaks crowd that region of the spectrum

that their effect is hard to estimate. These interferences include the Sm^{153} .0754 and .0834 MeV peaks. Baseline placement is uncertain, and varies with the Ho/Sm ratios of the samples and standards. Only the top 3 channels of the Ho^{166} .0806 MeV peak are used in order to reduce the effects of systematic baseline error. Statistical uncertainties are $\pm$ 5% or more.

Erbium

Two relatively small peaks from Er^{171} appear in the first count set. One of these, .3084 MeV, is used to obtain an approximate value for Er. The peak is free from interferences, but rests on a relatively high Compton tail, mostly from Eu^{152m}, so that the statistical uncertainties range from $\pm$ 15% up.

Thulium

The single, weak Tm^{170} peak at .0843 MeV shows up in count set IV as a shoulder on the Tb^{160} peak at .0866 MeV. One of our detectors partially resolves those peaks, so that a Tm value with an uncertainty of $\pm$ 15-20% could be obtained. Because of the similarity in geochemical behavior of Tm, Yb, and Lu and the much more precise values normally obtained for those elements, we do not consider a Tm value of that accuracy worth the effort required to obtain it.

Ytterbium

Usable peaks are obtained from two isotopes, Yb^{175} (.2826 MeV) and Yb^{169} (.1772 MeV) in count sets II-IV. Statistical uncertainty for Yb^{175} (.2826 MeV) in count set III, the most favorable, is about $\pm$ 4% for basalts. The peak is completely free from any known interference. The .1772 MeV peak from Yb^{169} is analyzed from count set IV after its only known interference, the .1729 MeV Sm^{153} peak, has decayed away. Statistical uncertainties for basalts are about $\pm$ 6%.

Lutetium

The .2084 MeV peak of Lu^{177} is prominent in count sets II-IV, and has a statistical uncertainty below $\pm$ 2% in set III for basalts. It can be used in sets II and IV for a consistency check.

The peak is surrounded by the .2156 and .1970 MeV peaks of Tb^{160}, but to a small enough extent that the uncertainty in the baseline is a fraction of a percent, well within the statistical uncertainties.

Geometry Effects

The greatest spurious cause of systematic error in our analysis appears to be irreproducibility of sample and standard monitor counting geometry. The oxalate precipitates prepared for counting are uniform in diameter and thickness. The cards they are mounted on fit snugly into the sample holders of the detectors. In order to obtain reasonable counting efficiency for count sets III and IV, however, the samples must be placed to within about 3 cm. of the detector faces. Displacement of the sample by 0.8 mm. toward or away from the detector relative to where the standard was counted produces, at that distance, a change in solid angle geometry of about 6%. This value is well outside the uncertaintly due to counting statistics for most of the REE. This estimated change was verified by carefully moving a Cs^{137} source away from the detector face and determining the observed photopeak activity as a function of distance. The rate of geometry change with distance decreases with the distance from the detector, but for a given count duration, the statistical uncertainty increases with that distance. Denechaud (1969) shows that low activity samples are best counted at a distance from the detector such that statistical uncertainties are 2-4 times greater than uncertainties due to sample position. This corresponds to about 3 cm. for the samples analyzed in this work, since positioning is accurate to better than 0.5 mm.

A test of sample preparation and counting was made by precipitating as oxalates batches of RE carrier with Y^{88} traces added. At 3 cm. from the detector face, variations in positioning for the individual samples were of the order of tenths of a percent, while variations in precipitation and mounting were of the order of a percent.

Occasionally, a sample is displaced sufficiently, however, that a geometry error of a few percent results. This is apparent from disagreement in the consistency checks, for example, Yb^{169} and Eu^{152} yielding values 4% lower in the fourth count set than found from

Eu^{152m} in set I and Yb^{175} in set III. In such a case, values for all elements in count set IV would be corrected for the geometry change. The reasons for these infrequent errors in geometry have not yet been discovered. Such errors occur only in values from count sets III and IV, for which the samples are counted close to the detector.

Testing showed that lateral movement of the sample of the order of 1 mm. produced no significant change in count rate, even for samples only 3 cm. from the detector face.

Determination of Chemical Yields

While 100% recovery of the carrier that is added to samples before their dissolution was not expected, it was hoped that losses of the individual REE would be uniform, i.e., if 20% for Sm, then 20% for La and Lu as well. If so, the REE could be titrated to get their combined yields before or after radioassay, and the percent individual element recoveries would be the same as the percent combined recovery. Combined recoveries ranged mostly from 70 to 90%. In the worst instances, however, 95% of the Sm might be recovered, but less than 50% of the La and less than 60% of the Lu, with a smooth variation in relative yield with atomic number, but no reproducibility from sample to sample. The newer chemical procedure outlined previously removes nearly all this variation, but unless and until extended experience with it gives us full confidence in its unfailing reproducibility, we will continue determining chemical yields by reirradiating portions of the samples and standards after count set IV has been completed.

As long as the combined yield is known from EDTA titrations, only relative elemental yields need to be determined by reirradiation, thus eliminating the need for weighing the portion of sample that is reirradiated or for iron wire flux monitors. Small uncertainties in counting geometry and small amounts of neutron self-shielding are unimportant. Advantage is taken of the smooth variation of chemical yield with RE atomic number, and a single count of the sample eight days after reirradiation is sufficient. Values are obtained directly for La, Sm, Eu, Tb, Yb, and Lu, and the rest are obtained by interpolation on a plot of relative chemical yield

(La(sample)/La(standard), etc.) versus atomic number. Uncertainties are less than $\pm$ 1% except for Ce and Nd which in the most severe cases of fractionation are uncertain to $\pm$ 3-4%. With the new chemical procedure, uncertainties are well below a percent for all elements.

The reirradiation time for the samples must be long enough that any residual activity from the initial irradiation for the elements being sought is negligible. From the compositions given in Table 1, it is seen that the relative amounts of Eu and Tb (the longest-lived radioactivities are from there) in the carrier relative to the samples or standard are about 750:1. By reirradiating for the same time and at the same flux as in the primary irradiation, the residual activity does not contribute significantly to the total. To avoid production of inconvenient levels of activity, less than 10% of each oxalate precipitate is reirradiated. A 50-minute count is then adequate to provide good counting statistics for all elements (more than 20,000 counts).

For the reirradiation, the necessary portions of the oxalate precipitates are spread thinly on 2.5 cm^2 circles of filter paper and held in place with Krylon 1302 spray coating. Each filter circle is then sealed between thin sheets of polyethylene by using a soldering gun. These sheets are mounted onto counting cards after the reirradiation.

The same peaks are used for chemical yield determination as for the original analysis. Competition from the .1032 MeV Gd^{153} peak contribute significantly to that same peak from Sm by the fourteenth day after reirradiation, so counting must be done before that. Counting cannot begin before the end of the seventh day because of contributions of Eu^{152m} to the peaks of Eu^{152}.

Calculation of individual RE chemical yields is done as follows:

Let k = normalization factor

l_i^c = milliequivalents of i^{th} lanthanide in added carrier

L^c = total milliequivalents of lanthanide in added carrier

l_i^s = milliequivalents of i^{th} lanthanide in sample precipitate

L^s = total milliequivalents of lanthanide in sample precipitate

V' = volume of EDTA solution required to titrate sample precipitate

N = normality of EDTA solution

y_i = chemical yield for lanthanide i

a_i^c = detected activity (peak area counts per unit time) of i^{th} lanthanide in carrier from fractionation-free precipitation of standard

a_i^s = detected activity of i^{th} lanthanide in carrier from precipitation of sample (corrected to time of standard count)

$$L^c = \sum_i 1_i^c$$

$$L^S = \sum_i 1_i^s = (V)(N)$$

$$\frac{1_i^s}{1_i^c} = \frac{a_i^s}{a_i^c} k = y_i$$

$$L_s = \sum_i 1_i^s = \sum_i y_i 1_i^s = \sum_i (k \frac{a_i^s}{a_i^c} 1_i^c) = k \sum_i (\frac{a_i^a}{a_i^c} 1_i^c) = (V)(N)$$

$$k = \frac{(V)(N)}{\sum_i (\frac{a_i^s}{a_i^c} 1_i^c)}$$

Thus, calculation of the normalization factor for a sample requires knowledge of the volume and normality of EDTA needed to titrate it, of the composition of the carrier solution, and of the relative yield numbers (a_i^s/a_i^c) read from the graph. Individual chemical yields are then obtained from the product $k(a_i^s/a_i^c)$.

Before the area under a gamma ray peak can be determined accurately, the baseline, usually do to the sum of Compton tails from several gamma peaks at higher energies, must be established. This requires an accurate graph of the pertinent part of the spectrum, i.e., counts per channel versus channel number. Graphs of sufficient accuracy are obtained with our point plotter described in an earlier section (Apparatus). The location of the energy center

of the peak to be summed is first estimated to the nearest third of a channel from the plot and the digital printout. A check for peak broadening due to analyzer drift is then made as follows. The peak channels determined fro two intense peaks in the spectrum are compared for all the spectra (samples and standard) of a count group. If the peak channels of consecutively counted samples do not differ by more than $^2/_3$ channel for both peaks, no significant scale shift has occurred. If a scale shift is indicated, half widths for the peaks are estimated to the nearest $^1/_3$ channel to determine whether the scale shift occurred at a time that caused significant peak broadening (i.e., during the middle $^3/_4$ of the count). If peak half-widths do not differ by more than 7%, "half peak" calculations as described below can be safely used; if more than 7%, "whole peak" calculations are necessary.

Peak broadening that requires whole peak calcualtions also occurs when analyzer dead time exceeds the limits given in the section on Apparatus.

Baseline contributions to peak channels are estimated by drawing smooth curves through the data points in the valleys surrounding the peak, then a baseline tangent to them. The baseline value directly under the determined center of the peak is then multiplied by the number of peak channels to be summed. This product is then subtracted from the sum across the selected peak channels.

The percent uncertainty in placement of the baseline is then estimated by considering the range over which reasonable baselines could be drawn on the graph. In the worst cases, the percent uncertainty is about equal to the statistical uncertainty for the baseline contribution to a single channel. This occurs when the peak being summed is barely resolved from other peaks on both sides. At best the percent uncertainty is about the same as the statistical uncertainty in the combined baseline contribution to 4 or 5 channels.

It is the uncertainty in placement of the baseline that makes half peak calculations worthwhile. The error in baseline placement has a much smaller effect on those channels for which the contribution from the baseline is a small fraction of the total, and such is never the case near the edges of a peak. Its effect is least on

the peak channel. Use of only the peak channel, however, increases the statistical uncertainty in the gross count and enhances the possibility for error due to indetectable analyzer drift. The optimum percent uncertainties for net peak counts occur when the uncertainty in the baseline and the statistical uncertainty in the gross counts are about equal. This occurs approximately when the number of channels summed corresponds to the full width at half maximum height (FWHM) of the peak. This number of channels is thus used except in the few cases where peak broadening has occurred. When peak broadening has occurred, a skewed peak shape may result, and the fraction of the total peak area in the channels above FWHM do not necessarily represent the same fraction of the counts as they do in an unbroadened peak. In these cases, whole peak calculations are required for both the affected sample(s) and standard.

The net peak counts, then, are the difference between the summed gross counts in the selected channels and the estimated baseline contribution. The error in the net peak counts is obtained by treating both the statistical uncertainty in the gross counts and the estimated uncertainty for the baseline as standard deviations. These uncertainties are propagated throughout the calculations (corrections for differences in counting times, comparisons between samples and standard monitors, etc.) as standard deviations.

Once the net peak counts and their uncertainties have been established, element concentrations are calculated, based on each peak summed, as follows.

$$c^s = \left(\frac{a^s}{a^o}\right) c^o \left(\frac{w^o}{w^s}\right) \left(\frac{f^o}{f^s}\right) \left(\frac{1}{y}\right)$$

c^s = concentration of sample in parts per million

c^o = concentration of standard in parts per million

a^s = peak area counts per unit time for sample (corrected to time of standard count)

a^o = peak area counts per unit time for standard

w^s = weight of irradiated sample in grams

w^o = weight of irradiated standard in grams

f^s = flux monitor counts per unit time for sample (corrected to time of standard count)

f^o = flux monitor counts per unit time for standard

y = chemical yield

Only for Dy, as previously discussed (Isotopes and Gamma Lines), do the results for a given element based on different peaks fall outside the range expected on the basis of the uncertainties calculated as described above. When several values for an element have similar uncertainties, an arithmetic average is taken to get a single value for the sample, and the uncertainties are propagated as standard deviations through the averaging process. When several values for an element have significantly different uncertainties, the value with the lower uncertainty is used to represent the sample, provided that the two values agree within their uncertainties; otherwise an average is taken as above.

Some results obtained by members of our research group using this method are given in Table 6. The basalt and troctolite were irradiated for 0.5 hr. at a flux of 1.3×10^{13} n/cm^2/sec. The feldspar concentrate was irradiated for 6 hours, the chondrite for 11.3. The sensitivity of the method is illustrated by the quantities of the various REE actually present in the irradiated samples. For the feldspar, these range from 0.5 to 200 nanograms, yet the statistical uncertainties are mostly less than 10%. Longer irradiations substantially enhance the accuracy for samples like the basalt and troctolite. We are now using 2 hour irradiations for routine work with such materials.

The work in this section was done by L. A. Haskin and E. B. Denechaud.

Table 6: Results Obtained With This Procedure

	BASALT AD-11			TROCTOLITE M6992			BRUDERHEIM CHONDRITE GS-13			FELDSPAR CONCENTRATE		
	ppm	standard deviation (± %)	micrograms in sample	ppm	standard deviation (± %)	micrograms in sample	ppm	standard deviation (± %)	micrograms in sample	ppm	standard deviation (± %)	micrograms in sample
La	12.1	1.7	4	1.27	3.1	1	1.23	3	.5	1.93	2	.17
Ce	27.6	2.2	9	2.09	3.3	2	3.64	1	1.5	2.26	2.5	.20
Nd	25	20	8	---	---	---	1.11	20	.5	0.59	10	.05
Sm	6.18	1.8	2	.245	1.2	.25	.143	1.5	.06	.106	2	.01
Eu	1.90	.53	0.6	.433	.47	.4	.063	2	.03	.606	2	.06
Gd	7.0	13	2	.26	19	.25	.43	8	.15	.18	10	.02
Tb	1.26	2.4	.4	.035	29	.03	.044	10	.02	.020	10	.002
Dy	8.7	10.3	3	.27	14	.25	.33	6	.15	.108	5	.01
Ho	1.61	5.0	.5	.046	15	.05	.060	5	.025	---	---	---
Er	3.8	13	1	---	---	---	.28	20	.1	---	---	---
Yb	3.69	4.6	1	.140	14	.15	.170	2	.07	.047	10	.004
Lu	.53	1.9	.2	.0157	6	.015	.031	3	.01	.0055	5	.0005

REE in the Stretishorn Dike

Introduction:

The Stretishorn dike is a composite dike in Eastern Iceland. It consists of 12 and 5 meter wide flanks of tholeiitic basalt and an 8 meter wide rhyolite core. These major materials are separated from each other by bands of hybrid rock whose composition grades from andesitic to rhyodacitic and whose widths nowhere exceed 2.5 meters. Extensive geochemical studies on major and minor elements have been recently reported by Gunn and Watkins (1969). These studies were made on cores taken at approximately one foot intervals across the face of the dike by Watkins, who has generously furnished us portions of some of them.

We have determined the REE in seven of these cores from the wider basalt flank and hybrid zone well into the rhyolite. The results bear on 3 of the conclusions reached by Gunn and Watkins, summarized below. The reader is referred to their paper for presentation of the evidence behind these conclusions as well as for a discussion of and further references to the geologic and petrographic description of the dike (Gunn and Watkins, 1969).

The pertinent conclusions are as follows:

1) The basalt of the flanks had been contaminated with about 10% of the rhyolite prior to emplacement of the dike.

2) The hybrid rocks correspond to simple mixtures of the "end-number" basalt and rhyolite now making up most of the dike. (A few minor elements, e.g. Pb and Zn, were found to deviate from the otherwise apparently linear mixtures.)

3) The rhyolite appears to be the fractionation product of a basaltic parent.

Results and Comparisons with Other Materials.

The analyses were done by the method described in the preceding section of this report. The analytical results are given in Table 7 . The relative RE abundances are identical for the 3 basalt samples, AD-80, AD-24, and AD-11, well-spaced across the basalt flank. The absolute abundances of AD-24 and AD-11 are

Table 7: REE in the Stretishorn Dike (ppm)

	AD-1	AD-6	AD-11	AD-24	AD-35	AD-47	AD-80 (II)
La	19.0±.2	11.3±.2	12.1±.2	11.9±.2	11.3±.2	12.4±.2	11.9±.3
Ce	45.2±.8	28.4±.7	27.6±.6	27.6±.7	35.4±.8	41.2± 1.0	21.2± 1.0
Nd	36± 7	28± 6	25± 5	27± 5	28± 4	34± 6	36± 8
Sm	11.9±.2	8.22±.09	6.18±.11	6.44±.16	9.80±.11	12.6±.3	5.62±.06
Eu	.95±.01	1.32±.02	1.90±.01	1.93±.02	.804±.008	1.02±.01	1.63±.02
Gd	13.9± 1.0	9.7± 1.5	7.0±.9	8.7± 1.4	11.4±.9	15.6± 2.3	4.1± 1.5
Tb	2.47±.04	1.82±.04	1.26±.03	1.39±.03	2.79±.03	3.72±.03	1.20±.05
Dy	19.0± 1.8	13.2±.3	8.7±.9	7.91±.66	15.4± 1.0	21.2± 1.1	7.25±.27
Ho	3.81±.14	2.46±.11	1.61±.08	1.61±.10	3.55±.29	4.48±.20	1.71±.24
Er	13.4± 2.0	10± 6	3.8±.5	-----	11.8± 1.8	13.8± 2.9	-----
Yb	9.46±.30	6.94±.23	3.69±.17	3.91±.13	9.10±.25	12.4±.4	3.54±.21
Lu	1.37±.01	.95±.02	.53±.01	.55±.01	1.28±.01	1.57±.02	.49±.02

also identical, while those for AD-80 are 10% less. The absolute concentrations for these were averaged, and this average is compared with that of the chondrites in the usual way in Figure 5 . The relative RE abundances for the rhyolite samples, AD-35 and AD-47, are similar but not quite identical, the light REE being a few percent more abundant in AD-35. The absolute RE abundances of AD-35 average about 20% less than those in AD-47.

There are no significant differences in the major element compositions among the basalts (Gunn, private communication). Rhyolite AD-47 has more than twice the CaO and only a third the MgO content of AD-35. The reasons for the variations in absolute RE contents within the rhyolite and basalt groups are unknown, but might be related to relative mineral abundances. (Modal analyses cannot be readily made on the exact fragment of the core used for analysis.) Variations of this magnitude in minor element content for rock chips from the same body are not uncommon. It is interesting to note that relative RE abundances are much less variable than absolute RE abundances.

The rhyolite contains xenocrysts of basalt of all sizes (Gunn and Watkins, 1969). The absolute RE abundances of the basalt are mostly less than those of the rhyolite, so contamination of AD-47 with a few percent of basalt might be expected to give the lower absolute RE abundances found in AD-35. This is untenable, however, since the Eu content of the basalt is approximately twice that of the rhyolite, and a difference in relative abundance for that element between the two rhyolites would necessarily result. Both samples of rhyolite have the same relative Eu deficiency, with only 22% of the Eu content "expected" from interpolation of the comparison diagrams (Figure 5).

The relative and absolute RE abundances in the basalt portion of the dike resemble those found by Schilling and Winchester (1966) for Hawaiian tholeiites and those found for diabases by Philpotts and Schnetzler (1968) and by Frey et al. (1968). There is a slight deficiency of Eu (down to 87% of the value expected from interpolation of Figure) and probably a slight deficiency of Ce. The absolute abundances of the heavy REE is in the range

Figure 5. Comparison Diagram for Stretishorn Basalt and Rhyolite

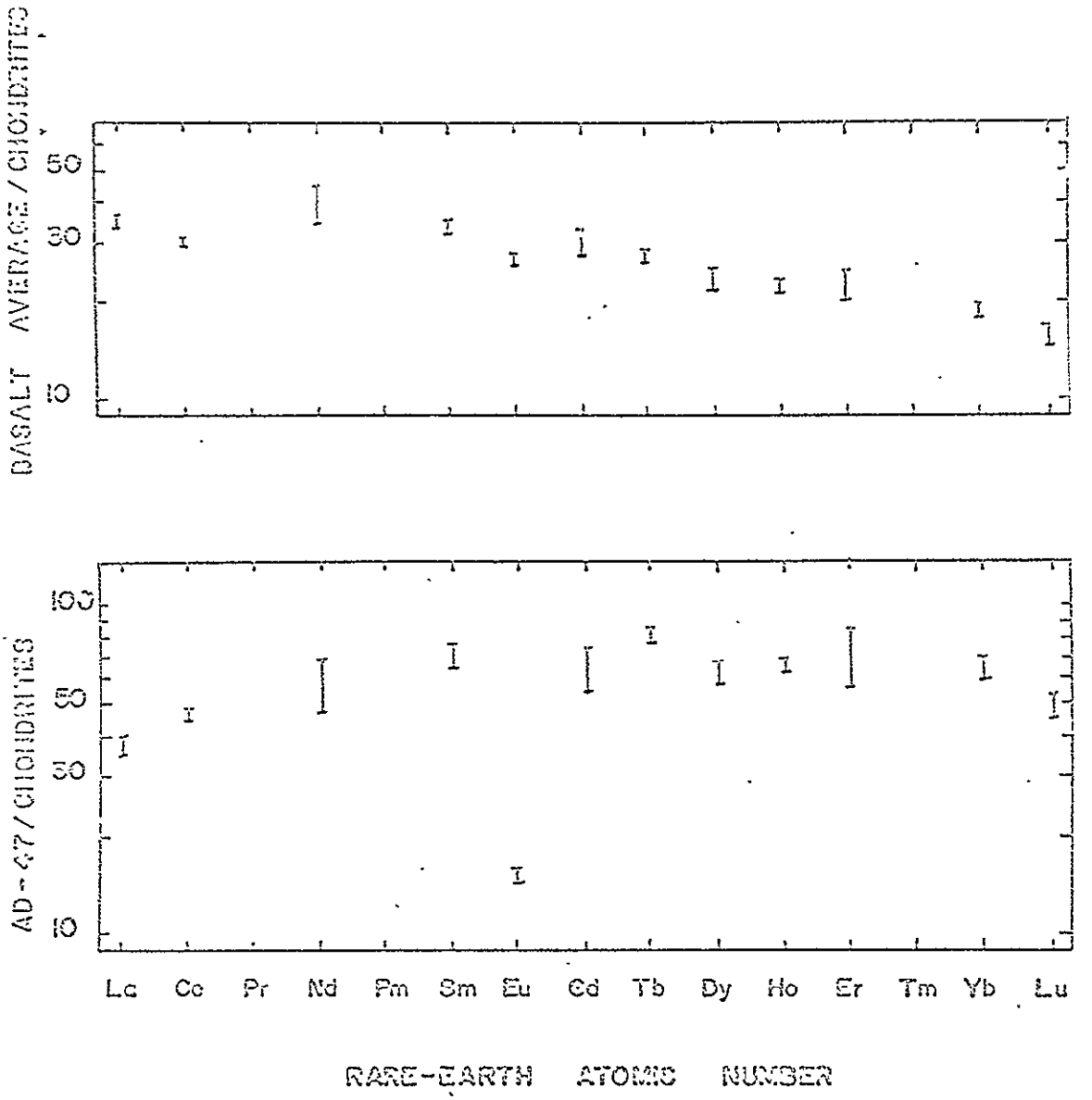

found for subalkaline marine basalts from the mid-Atlantic ridge, but these have much lower light RE abundances than the Stretishorn basalt (Frey et al., 1968).

The Stretishorn rhyolite has very different relative and absolute abundances from a composite of rhyolites from continental locations (Haskin et al., 1968) and which is the only sample of rhyolites for which literature analyses are presently available. Both are deficient in Eu, however. A trachyte from the Hawaiian Islands (Schilling and Winchester, 1966) has a minimum in its comparison diagram (relative to chondrites) at about Gd, and no Eu anomaly. A trachyte from Gough Island (Frey et al., 1968) has much higher light RE abundances than the Stretishorn rhyolite, and a much larger Eu deficiency (only 7% of the interpolated value!). A soda trachyte from Ascension Island is also deficient in Eu (57% of interpolated value) but, relative to chondrites, is strongly enriched in the light REE. Except for the large Eu anomaly, the relative RE abundances in the rhyolite most closely resemble those found for subalkaline marine tholeiites (Frey et al., 1968).

There is, curiously, an apparent Tb anomaly in the rhyolites. Tb seems to be enriched to about 1.19 times the interpolated value. No firm evidence for a Tb anomaly has previously been shown, and none has been expected. Tb can, by loss of 4 electrons, obtain a half-filled subshell; this occurs to a degree when Tb is oxidized in air to Tb_4O_7. Attainment of that configuration is invoked to explain the anomalous behavior of Eu (for example, Haskin and Frey, 1966).

Our first inclination was to treat the anomaly as an analytical artifact. However, the rhyolite samples were analyzed in separate runs, and in both cases along with other samples which show no Tb anomalies. The only element whose ratio to Tb varies significantly among the samples for those runs is Eu. Eu is very low in the rhyolites, and an undetected interference from it would lower, not raise the Tb value. Considerations of background line error and the Tb/Eu ratio in the standard and other samples also lead to Tb deficiencies, not excesses, for the rhyolites. Thus, the possibility of a real Tb anomaly has not been removed. A similar

anomaly was observed in a single sample of the Ramsdorf chondrite (Haskin et al., 1968).

Discussion:

1) Contamination of the basalt portion by ~10% of the rhyolite prior to intrusion. The principal evidence for this includes xenocrysts of inverted tridymite, variation in K_2O and SiO_2 contents from core to core, antipathetic variation between Ca and Na despite a constant concentration of plagioclase, and antipathetic variation between Na and Sr (Gunn and Watkins, 1969).

Gunn and Watkins also point out that the chilled basalt from the outer edge of the dike is lower in K_2O, SiO_2, and Na_2O compared with the average Stretishorn basalt, and they refer to this chilled basalt as being the least contaminated by the rhyolite. Apparently, however, the basalt flanks had more or less solidified before the rhyolite was intruded, so contamination of the basalt by the rhyolite had to occur before its intrusion. That being so, it is difficult to regard the chilled basalt margin as original basalt that escaped contamination by the rhyolite. We suggest that the chilled margin instead is contaminated with some of the basalt against which it chilled, and whose composition could very likely be that needed to account for the differences in composition between the chilled margin and the other Stretishorn basalt samples.

If we assume that the basalt was contaminated with about 10% rhyolite prior to intrusion, we can estimate its original RE abundances by subtracting from the average basalt RE content 10% of the average rhyolite content and multiplying the result by 10/9. The resulting absolute and relative abundances (Table 8) for the basalt are not greatly different from those actually found in the basalt, except for Eu, which is so depleted in the rhyolite. It is interesting to note that, when the above "correction" is made, the small Eu deficiency in the Stretishorn basalt disappears.

This is not necessarily significant, but it is worth noting that basalts commonly do not have Eu anomalies, whereas more acid rocks, as a rule, do (Haskin et al., 1966; Frey et al., 1969;

Table 8: RE abundances in Stretishorn basalts after "correction" for rhyolite (column 1) and percentage basalt in hybrid AD-6 (column 2)

La	-----	-----
Ce	24.4±.5	.85±.35
Nd	23± 3	-----
Sm	5.57±.08	.59±.32
Eu	1.96±.01	.44±.14
Gd	6.7±.8	.62±.44
Tb	1.06±.02	.73±.28
Dy	6.9±.5	.50±.32
Ho	1.26±.09	.63±.22
Er	3.5±.7	-----
Yb	2.89±.11	.55±.26
Lu	.42±.01	.52±.16

Philpotts and Schnetzler, 1968). At the very least, the disappearance of the Eu anomaly for the basalt is an interesting coincidence.

2) The hybrid rocks as simple linear mixtures of the basalt and rhyolite constituents of the dike. This is well established by Gunn and Watkins (1969) who showed that the concentrations for most of the elements determined, when plotted versus SiO_2 content, or various indices of basicity or differentiation, produced straight lines. Processes of secondary importance are then required to explain deviations for a few trace elements. The REE are not generally thought of as mobile. Strong weathering of subalkaline marine tholeiite to greenstone has apparently not affected their absolute or relative abundances (Frey et al., 1968).

Figure 6 is a graph of concentration versus distance across the dike for 7 of the REE. The concentrations of Yb and Lu, examples of heavy REE, are fairly steady across the basalt, rise through the transition, and are much higher in the rhyolite. Eu, which has higher concentrations in the basalt than in the rhyolite, displays the opposite trend. La has the same concentration in the basalt and rhyolite, but La, Ce, and Sm have anomalously high concentrations in AD-1 at the rhyolite edge of the transition zone. The reasons for this anomaly are not known, but some kind of fractionation of the REE has accompanied the mixing of the rhyolite and basalt when the hybrid rocks formed, and the lightest REE were the most affected.

Hybrid rock AD-6, at the basalt edge of the transition zone, is the most different in RE concentrations from the rhyolite and basalt, and is therefore most suited for a test of linear mixing. The percent of basalt and rhyolite in the presumed mixture (AD-6) can be calculated for each of the REE. The results of this calculation appear in Table 8 . The average for AD-11, 24, and 80 was used for the basalt and the average of AD-35 and 47 for the rhyolite. The standard deviations listed in Table are large because of the uncertainty of absolute contents of the REE in the rhyolite. La was not used because the concentrations in the basalt and rhyolite are the same. For the same reason, the error in the Ce value is large. Nd and Er were not used because their analytical uncertainties are too big. The fraction of basalt in the mixture

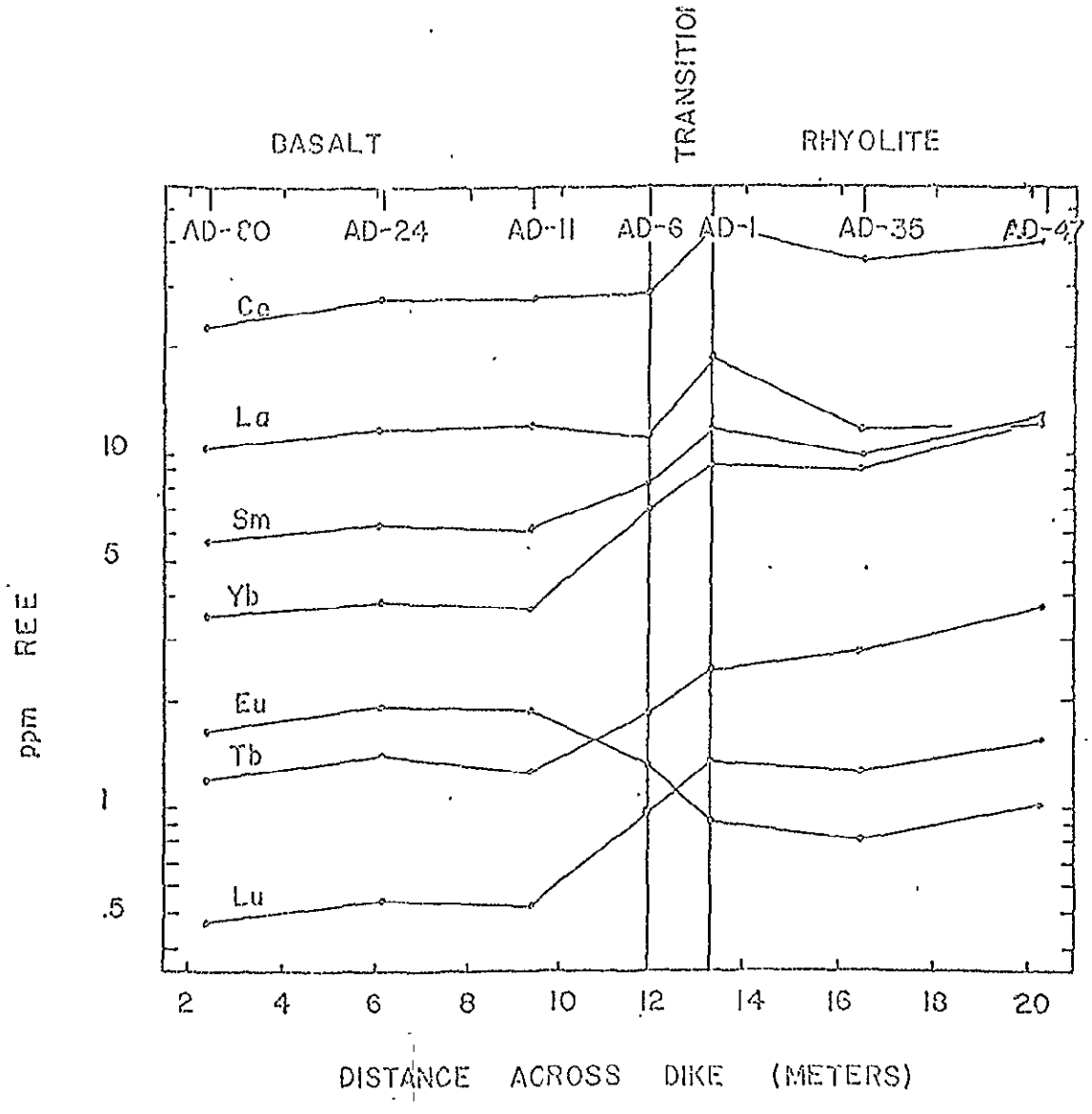

Figure 6. Concentrations of several REE as a Function of Distance Across the Dike.

for the remaining 8 REE ranges from .44 to .73, and the narrower range of .45 to .58 is within the estimated uncertainties for all 8 results. The abundances of these elements, then, are consistent with the production of AD-6 by mixing rhyolite and basalt in approximately equal amounts. By making the same calculation for the major elements, using data of Gunn (private communication) we get a range of 50 to 57% basalt.

AD-6 can be tested to see whether its relative RE abundances correspond to a linear mixture of the relative RE abundances of the basalt and the rhyolite. This is a more precise test for the REE than that based on absolute abundances because the uncertainties in relative abundances for the basalt and the rhyolite are lower than those for the absolute abundances. Denechaud (1969) has done these computations. The most precise value for the fraction of basalt in the mixture (corrected for absolute abundances after the calculation) is that for Eu, $0.47 \pm .05$.

Thus, most of the RE contents in AD-6 are consistent with formation of that rock by simple mixing of rhyolite and basalt.

3) The rhyolite as a fractionation product of basaltic magma. As noted earlier, the relative and absolute RE abundances for the few other acid volcanic rocks thought to have possibly been produced by differentiation of basic magma are quite different from those in the Stretishorn rhyolite. Models for fractional crystallization are known (see, for example, McIntire, 1963) that can be applied to the present case. Schnetzler and Philpotts (1968) have derived partition coefficients between basaltic magma and several rock forming minerals. These are supported by measurements of Onuma et al. (1968) and Frey (1969).

The only mineral known to incorporate anomalous amounts of Eu is feldspar (for example, Towell et al., 1965; Haskin et al., 1966; Philpotts and Schnetzler, 1968). No mechanism for producing Eu anomalies other than selective incorporation into feldspar has any experimental support. It is instructive to apply the logarithmic law of trace element partition and the RE partition coefficients to generate the Eu anomaly found in the Stretishorn rhyolite.

We begin with equations (45) from McIntire (1963).

$$C^L = C^S/\lambda = C^A(1-x)^{\lambda-1}$$

Here, C^L is the concentration of the trace element in the crystallizing liquid, C^S the concentration in the solid, C^A the average concentration for all the solid plus liquid, x the fraction of liquid solidified and λ the partition coefficient. This equation can be written for Eu, and independently for another REE, say Sm. The ratios of concentrations of these elements and their relations to the above equation become $C^L_{Eu}/C^L_{Sm} = 1.02/12.6$, the ratio of Eu to Sm in rhyolite AD-47, taken to be the residual liquid from crystallization, and $C^A_{Eu}/C^A_{Sm} = 1.90/6.2$, the ratio of Eu to Sm in basalt AD-11, taken to be the initial liquid to be differentiated. λ_{Eu} and λ_{Sm} are 0.35 and 0.10 for feldspar, according to Schnetzler and Philpotts (1968).

X, then, is the fraction of the initial basaltic liquid that would have to crystallize as feldspar to give a residual liquid with the Eu/Sm ratio of the rhyolite.

$$\ln(1-x) = \frac{1}{\lambda_{Eu} - \lambda_{Sm}} \ln\left[(C^L_{Eu}/C^L_{Sm}) - (C^A_{Sm}/C^A_{Eu})\right]$$

This gives the impossible result that 99.5% of the basalt would have to crystallize as feldspar. This result is not appreciably affected by changes in the starting basalt composition that are in the range for known basalts. Acknowledgement of the precipitation of pyroxene, olivine, or other minerals that would also be crystallizing but that do not selectively incorporate Eu, drastically raises the fraction solidified. It is seen from the above equation that the difference between the partition coefficients for Sm and Eu is the major factor for providing a rapid change of Eu/Sm ratio with percent crystallization of the melt. In order to provide the observed Eu/Sm ratio in the Stretishorn rhyolite from a basalt liquid by the above process before 90% of the liquid had crystallized would require $(\lambda_{Eu} - \lambda_{Sm})$ to be 0.6. The largest difference we have ever observed is a tentative value of 0.5 for a feldspar in the Skaergaard intrusion (Paster and Haskin, unpublished result) and that would require 93% of the basalt liquid to crystallize as feldspar, still clearly impossible.

Alternatively, the rhyolite would have to be the microscopic end product of fractionation of many orders of magnitude its volume of original liquid (e.g., for $\lambda_{Eu} - \lambda_{Sm} = 0.1$, $x = 0.999998$).

These results do not support the hypothesis that the rhyolite is the product of the differentiation of a basaltic liquid. On the other hand, they do not particularly refute it, since the present model suggests that none of the really large Eu anomalies observed in nature can be generated from any reasonable starting material. Either the model is incomplete or wrong, or the partition coefficients are. Models based on fractional melting or zone refining would also need much larger differences of partition coefficient between Sm and Eu than are supported by direct evidence to generate the ratios found in nature.

The work in this section was done by E. B. Denechaud and L. A. Haskin.

Multielement Activation Analysis with Group Separations

An analytical procedure designed to increase the information available on precious samples that must be destroyed for RE analysis was discussed in our previous report. Development of the method has continued and, while further minor modifications are desirable, the present scheme reliably yields useful data for up to 40 elements. During its development, we have used it for analysis of 6 whole-rock chips and on separated mineral phases from the Bruderheim chondrite. Precision has improved steadily, except where new innovations did not work out as expected. The actual analytical results are presented in the next section of the report.

There are now 12 element groups, of which 4 are single elements. Separate standard monitors are included for each element group except VIII and X, for which a single monitor is adequate, and VI, for which the Fe wire used to correct for flux gradients also serves as monitor. Stock solutions are prepared and standardized for each element, then diluted, and aliquots are pipetted into fused quartz irradiation capsules. The capsules are placed under a heating lamp to evaporate the solutions slowly, leaving the standards on their walls, then sealed for irradiation. We have had no difficulty recovering quantitatively the elements of interest after irradiation.

Carrier for each element to be determined is also prepared, usually from the same stock solutions. A complete set of carriers for all groups is pipetted and evaporated into a zirconium crucible in which the sample is to be fused. Identical portions of the carriers for each group are stored in 50 ml erlenmeyer flasks and, after irradiation, the standard monitor for each group is mixed with its carrier, which is then precipitated in the same manner as is that group from the sample.

Table 9 lists the concentrations of the standard solution, the weights of carrier used, and the compounds from which they are made. 1.0 ml of standard is used.

The chemical separations are done by Mr. Allen or by me. Three topnotch undergraduate chemistry majors assist with precipitation of standard monitors, filtering and mounting of precipitates, gamma spectrometry, and data processing. The sample is removed from the

reactor, typically, at about 1:00 pm. Except for Group XII, the alkali metals, which are left to precipitate overnight, the chemical separations are completed and the groups mounted for counting by about 9:00 pm. The times at which counting of each sample is done are included in Table 10.

Chemical yields are obtained by reirradiating the samples and standards after final radioassay and comparing the activities induced in the precipitated carriers. The compositions of the carriers have been adjusted to optimize this procedure. To facilitate chemical yield determination, the filter circles and precipitates are heat sealed between thin sheets of polyethylene before initial radioassay. These samples, then, can be easily removed for reirradiation, then remounted, still in their polyethylene sheaths, for chemical yield determination. Fe and Ni are titrated, not reactivated.

Data are processed by hand, as indicated for the REE in the first section of this report.

An up-to-date flow chart for the chemical procedures is included as Table 11.

The interferences due to other elements producing the nuclide of interest, given in Table 12, are based on the data of Lukens (1963) for a reactor with characteristics similar to ours.

The work in this section was done by R. O. Allen, L. A. Haskin, M. A. Anderson, J. W. Blackbourn, and K. A. Zweifel.

Table 9. Information on Standards and Carriers

Element and Group		gm/ml	Compound	Standardization	Carrier wt. (mg)
I	Ag	1.00	$AgNO_3$	direct weighing of $AgNO_3$	300
	Br	81.2	NH_4Br	gravimetric, AgBr-agreed to .2% of direct wt.	10
II	Au	.278	Au^o	weighed, diss. in aqua regia	3
	Ba	.102	$Ba(NO_3)_2$	titr. w. EDTA-phthalein complexane	30
	Pt	2.94	Pt^o	weighed, diss. in aqua regia (H_2PtCl_6)	12
	Ta	10.7	Ta^o	weighed, diss. in HF	15
III	Mn	928	$Mn(NO_3)_2$	titr. EDTA, eriochrome black T	10
IV	In	8.18	$In(NO_3)_3$	titr. EDTA, PAN	50
V	As	15.0	As_2O_3	direct weighing, diss. NaOH (Na_2AsO_4)	10
	Cu	63.2	$Cu(NO_3)_2$	titr. EDTA, PAN	50
	Pd	.0559	$Pd(NO_3)_2$	titr. EDTA, eriochrome black T	5
	Sb	3.87	$K(SbO)C_4H_4O_6$	direct weighing, diss. H_2O	6
	Se	10.0	$(NH_4)HSeO_4$	direct weighing, diss. H_2O	20
VI	Fe	-----	Fe^o	(60mg wire)	30
VII	La	11.2	nitrates	titr. EDTA, PAN	0.9
	Ce	7.92	nitrates	titr. EDTA, PAN	0.8
	Nd	14.3	nitrates	titr. EDTA, PAN	0.6
	Sm	.917	nitrates	titr. EDTA, PAN	0.6
	Eu	.389	nitrates	titr. EDTA, PAN	0.6
	Gd	4.79	nitrates	titr. EDTA, PAN	0.6
	Tb	.395	nitrates	titr. EDTA, PAN	0.6
	Dy	.921	nitrates	titr. EDTA, PAN	0.6
	Ho	.986	nitrates	titr. EDTA, PAN	0.6
	Er	3.82	nitrates	titr. EDTA, PAN	0.7
	Yb	1.00	nitrates	titr. EDTA, PAN	0.9
	Lu	.196	nitrates	titr. EDTA, PAN	0.9
VIII, X	Cr	100	$K_2Cr_2O_7$	direct weighing	30
	Hf	9.0	HfOCl	direct weighing	15
	Sc	17.8	$Sc(NO_3)_3$	titr. EDTA, PAN	10
	Th(Pa)	11.4	$Th(NO_3)_4$	titr. EDTA, pyrocatechol violet	--
	Co	27.8	$Co(C_2H_3O_2)_2$	titr. EDTA, pyrocatechol violet or murexide	10
	Ga	6.91	$Ga(NO_3)_3$	titr. EDTA, pyrocatechol violet	5
	Zn	71.5	$Zn(C_2H_3O_2)_2$	titr. EDTA, eriochrome black T	30
IX	Ni	10,800	$Ni(NO_3)_2$	titr. EDTA, PAN	20
XI	Ca	4,040	$Ca(NO_3)_2$	titr. EDTA, murexide	10
	Sr	410	$SrCl_2$	titr. EDTA, phthalein complexane	10
XII	Cs	2.4	$CsC_2H_3O_2$	direct weighing	5
	K	980	KHPhth.	direct weighing	(KNO_3)70
	Rb	91	$RbC_2H_3O_2$	direct weighing	20

Table 10. Separation groups and counting data.

Separation Group	Time of Count	Duration of Count	Energy Range Observed (MeV)	Isotope Observed	Gamma Peak Used (MeV)
I.	30 da	11 hr	1	Ag^{110m}	.658 .885 .937
	1 da	3 hr	1	Br^{82}	.554 .619 .698 .777
	3 hr	40 min	3	Cl^{38}	1.64 2.17
II.	3 hr 6 da	5.5 hr 11 hr	1 2	Au^{198}	.412
	6 da	11 hr	2	Ba^{131}	.124 .216
	3 hr	5.5 hr	1	Ba^{139}	.166
	3 hr	5.5 hr	1	Pt^{197}	.078
III.	1 da	20 min	3	Mn^{56}	.847 1.811 2.113
IV.	4 hr	1 hr	2	In^{116m}	.417
V.	1 da	5.5 hr	2	As^{76}	.559 .657 1.216
	1 da	5.5 hr	2	Cu^{64}	1.346
	1 da	5.5 hr	2	Pd^{109} Pd^{111m}	.088 .172
	5 da	2.5 hr	1	Sb^{122}	.564
	1 da	5.5 hr	2	Sb^{124}	.603
	5 da	2.5 hr	1	Se^{75}	.136 .265 .280

VI. See Section 1 of Report.

Separation Group	Time of Count	Duration of Count	Energy Range Observed (MeV)	Isotope Observed	Gamma Peak Used (MeV)
VII.	14 da	5.5 hr	2	Fe^{59}	.193 1.099 1.292
VIII.	7 da	11 hr	2	Cr^{51}	.320
	1 da	5.5 hr	2	Hf^{181}	.133
	7 da	11 hr	2		.482
	7 da	11 hr	2	Pa^{233}(Th)	.300 .312
	1 da	5.5 hr	2	Sc^{46}	.889
	7 da	5.5 hr	2		1.120
IX.	5 hr	1 hr	2	Ni^{65}	.367 1.115 1.481
X.	1 da	5.5 hr	2	Co^{60}	1.173
	7 da	15 hr			1.332
	1 da	5.5 hr	2	Ga^{72}	.630 .834
	1 da	5.5 hr	2	Zn^{69m}	.439
XI.	30 da	30 min		Ca^{45}	BETA
	12 hr	5.5 hr	2	Ca^{47}	.160 1.297
	12 hr	5.5 hr	2	Sr^{87m}	.389
XII	6 da		2	Cs^{134}	.605 .796
	1 da	2.5 hr	2	K^{42}	1.525
	6 da	11 hr	2	Rb^{86}	1.077

Table 11. Flow Chart

1. Fuse sample and carriers in Na_2O_2.
2. Digest fusion cake in 100 ml H_2O.
3. Acidify to pH = 1 with conc. H_2SO_4.
4. Centrifuge.

Solid A | Liquid A

Solid A:
1. Stir with 20 ml $NH_3(aq)$; centrifuge.
2. Repeat 1, combine supernates from 1 and 2

Liquid A → to next page

Solid B | Liquid B

Solid B:
1. Add 10 ml conc HNO_3.
2. Add $NaNO_2$ until reaction subsides; centrifuge.
3. Add Fe^{+++}, Sc^{+++}, Mn^{++} holdback carriers to solid.
4. Repeat 1 and 2, discard supernate.
5. Wash precipitate with H_2O, discard supernate.
6. Wash with ethanol, decant, filter from ether slurry

Solid C | Liquid C

Solid C:
Group II Au, Pt, Ba, Ta

Liquid B:
1. Add Mn^{++} and Sc^{+++} holdback carriers.
2. Acidify with HNO_3; centrifuge.
3. Dissolve precipitate in $NH_3(aq)$.
4. Centrifuge to remove MnO_2.
5. Repeat 2.

Group I Ag, Cl, Br

Liquid C:
1. Add $NH_3(aq)$ to supernate from step 2, solid B, to get MnO_2.

Group III Mn

Liquid A

1. Add 8 gm NaI per 100 ml solution.
2. Extract In with 25 ml diethyl ether. See note 1.
3. Repeat 2.

Ether phase D'

1. Wash with Fe^{+++} and Mn^{++} holdback solution containing NaI and H_2SO_4 to give 0.5 M HI.
2. Repeat 1.
3. Back extract with 20 ml 5 M HCl.
4. Repeat 3; combine aqueous phases.

Ether phase E'

1. Discard into special waste; I_2 present which could react to form NI_3

Aqueous phase D

1. Add H_2SO_4, $NaNO_2$ until no more I_2 forms.
2. Extract I_2 into 100 ml diethyl ether (Note 1)
3. Repeat 1.
4. Add H_2SO_4 to pH ~ 1, $NaNO_2$ to check for I_2 formation.
5. If necessary, repeat 2.
6. Discard ether phase into special waste as in E'-1.
7. Warm aqueous phase on hotplate, add urea to get rid of oxides of nitrogen.
8. Test 10 ml of soln. with H_2S gas; if S appears, repeat 7 and 8.
9. Bubble H_2S through solution
10. Add NH_3(aq) slowly, with stirring, to pH = 1.

1. Add NH_3(aq) to pH = 4.
2. Buffer with 6 M NH_4Ac (2 ml per 12 ml solution).
3. Add H_2S gas.
4. Filter off In_2S_3.

Group IV In

Solid F

1. Wash with H_2O, filter.

Liquid F

to next page.

Group V Cu, As, Se, Pd, Sb

Liquid F

1. Boil to remove H_2S, keeping pH≤ 1.
2. Test 10 ml with NH_3(aq); if precipitate forms, repeat 1.
3. Add NH_3 (aq) to pH = 8; centrifuge.

Solid G | Liquid G

1. Dissolve in conc. HCl.
2. Make solution 8 M in HCl.
3. Extract Fe in 20 ml diethyl ether. Note 1.
4. Repeat 3, combine ether phases.

Ether phase H' | Aqueous phase H

1. Add 20 ml H_2O.
2. Boil on hotplate to remove ether.
3. Add H_2S and NH_3(aq).
4. Filter precipitate.

Group VI Fe

1. Add NH_3(aq) to pH = 8.
2. Centrifuge, discard supernate.
3. Wash precipitate with dilute NH_3(aq).
4. Dissolve in minimum HCl; heat to 90° C.
5. Add 2 ml saturated aqueous oxalic acid.
6. If gelatinous precipitate of Zr oxalate forms, heat, add more oxalic acid, then NH_3(aq) dropwise until hard, crystalline rare-earth oxalates begin to appear.
7. Let cool to room temperature, centrifuge.

Solid I | Liquid I

Group VII Rare Earths

1. Bubble H_2S through solution.
2. Add NH_3(aq) to get black sulfide precipitate.
3. Centrifuge, rinse, discard supernates.

Group VIII Sc, Hf, Cr, Pa

Liquid G

1. Add Mn++ holdback carrier.
2. Filter out MnO_2.
3. Acidify with HCl to pH = 6.
4. Add alcohol solution of dimethylglyoxime.
5. Add NH_3(aq) slowly, with stirring, to pH = 8.
6. Heat to coagulate precipitate. Filter.

Solid J

1. Dissolve precipitate in 6 M HNO_3.
2. Triple volume of solution with H_2O.
3. Reprecipitate slowly with NH_3(aq) and dimethylglyoxime.

Group IX Ni

Solid K

Group X Co, Zn, Ga

Liquid J

1. Add NH_3(aq) to pH = 9.
2. Bubble in H_2S.
3. Boil to coagulate.
4. Filter

Liquid K

to next page

Note 1. At this point, the appearance of gelatinous silica may interfere with the extraction. Centrifuge to get an aqueous phase, an ether phase, and a semisolid silica phase. Wash the silica phase twice with dilute H_2SO_4, add the washings to the aqueous phase, discard the silica residue, and proceed.

Liquid K

1. Acidify to pH = 1-2.
2. Boil to expel H_2S.
3. Add saturated ammonium oxalate, NH_3(aq) to pH = 5-7.
4. Centrifuge.

Solid I

1. Slurry and filter.
2. Ignite, cool, dissolve ash in HCl.
3. Centrifuge and discard any solid impurities.
4. Add Na+ holdback carrier.
5. Add NH_3(aq) to pH 6, stir in saturated ammonium oxalate
6. Filter.

Group XI Ca, Sr

Liquid L

1. Add 10 gm NaOH pellets; 10 drops phenolphthalein.
2. Boil to expel NH_3.
3. Add NaOH pellets as needed to keep indicator pink.
4. When only $^1/_3$ the original volume remains, decant and discard crystallized sodium salts.
5. Add 5 ml 0.1 M EDTA.
6. Double the volume with formaldehyde.
7. Cool in ice bath to about $0^oC.$, decant and discard sodium salts.
8. Add sodium tetraphenyl boron reagent.
9. Let sit for several hours(warming to room temperature is all right).
10. Centrifuge, discard supernate.
11. Dissolve in minimum of acetone.
12. Reprecipitate with ethanol solution of tetraphenyl boron reagent.

Group XII K, Rb, Cs

Table 12. Contributions to Nuclide Production by Interfering Elements.

	Nuclide	(n,γ) parent	cpm/gm	(n,p) parent	cpm/gm	(n,∝) parent	cpm/gm	U(n,f) cpm/gm
I.	Ag^{110m}	Ag^{109}	1.5×10^{6}	Cd^{110}	5×10^{0}	In^{113}	<1	------
	Cl^{38}	Cl^{37}	3×10^{9}	Ar^{38}	1.2×10^{4}	K^{41}	3×10^{6}	------
	Br^{82}	Br^{81}	5×10^{9}	Kr^{82}	1.7×10^{5}	Rb^{85}	5×10^{4}	4×10^{3}
II.	Au^{198}	Au^{197}	8×10^{10}	Hg^{198}	2×10^{3}	------	------	------
	Pt^{197}	Pt^{196}	1×10^{8}	Au^{197}	1×10^{3}	Hg^{200}	1×10^{1}	------
	Ba^{131}	Ba^{130}	5×10^{6}	------	------	------	------	------
	Ta^{182}	Ta^{181}	1.2×10^{8}	W^{182}	5×10^{1}	Re^{185}	6×10^{3}	------
III.	Mn^{56}	Mn^{55}	5×10^{11}	Fe^{56}	3×10^{7}	Co^{59}	8×10^{6}	------
IV.	In^{116m}	In^{115}	3×10^{12}	Sn^{116}	1×10^{4}	------	------	------
V.	As^{76}	As^{75}	6×10^{9}	Se^{76}	8×10^{4}	Br^{79}	6×10^{4}	------
	Cu^{64}	Cu^{63}	6×10^{9}	Zn^{64}	3×10^{7}	------	------	------
	Pd^{109}	Pd^{108}	4×10^{9}	Ag^{109}	7×10^{4}	Cd^{112}	1.2×10^{2}	8×10^{5}
	Sb^{122}	Sb^{121}	3×10^{9}	Te^{122}	4×10^{3}	------	------	------
	Sb^{124}	Sb^{123}	5×10^{7}	Te^{124}	1.4×10^{2}	I^{127}	1.1×10^{2}	------
	Se^{75}	Se^{74}	3×10^{7}	------	------	Kr^{78}	5×10^{2}	------
VI.	La^{140}	La^{139}	5×10^{9}	Ce^{140}	3×10^{3}	------	------	1.1×10^{7}
	Ce^{141}	Ce^{140}	1.3×10^{8}	Pr^{141}	5×10^{3}	Nd^{144}	6×10^{2}	2×10^{7}
	Nd^{147}	Nd^{146}	9×10^{6}	------	------	Sm^{150}	5×10^{0}	1.9×10^{6}
	Sm^{153}	Sm^{152}	6×10^{10}	Eu^{153}	3×10^{4}	Gd^{156}	6×10^{1}	3×10^{7}
	Eu^{152m}	Eu^{151}	3×10^{11}	Gd^{152}	1×10^{2}	------	------	------
	Gd^{153}	Gd^{152}	1×10^{2}	------	------	Dy^{156}	<1	------
	Tb^{160}	Tb^{159}	3×10^{7}	Dy^{160}	1×10^{1}	------	------	------
	Dy^{165}	Dy^{164}	1×10^{12}	Ho^{165}	1×10^{5}	Er^{168}	1×10^{2}	------
	Ho^{166}	Ho^{165}	1×10^{11}	Er^{166}	8×10^{3}	Tm^{169}	2×10^{2}	5×10^{1}
	Er^{171}	Er^{170}	4×10^{9}	------	------	Yb^{174}	1×10^{2}	------
	Yb^{169}	Yb^{168}	1×10^{9}	------	------	------	------	------
	Yb^{175}	Yb^{174}	1.3×10^{9}	Lu^{175}	6×10^{2}	Hf^{178}	1×10^{1}	------
	Lu^{177}	Lu^{176}	7×10^{9}	Hf^{177}	2×10^{2}	Ta^{180}	1×10^{0}	------
VII.	Fe^{59}	Fe^{58}	1.4×10^{5}	Co^{59}	2×10^{5}	Ni^{62}	3×10^{1}	------
VIII.	Cr^{51}	Cr^{50}	2×10^{7}	------	------	Fe^{54}	1.3×10^{3}	------
	Hf^{181}	Hf^{180}	1.1×10^{8}	Ta^{181}	3×10^{2}	W^{184}	1×10^{1}	------
	Pa^{233}	Th^{232}		------	------	------	------	------
	Sc^{46}	Sc^{45}	7×10^{8}	Ti^{46}	5×10^{4}	------	------	------
IX.	Ni^{65}	Ni^{64}	8×10^{7}	Cu^{65}	9×10^{5}	Zn^{68}	1.4×10^{5}	------
X.	Co^{60}	Co^{59}	1.5×10^{7}	Ni^{60}	4×10^{2}	Cu^{63}	8×10^{2}	------
	Ga^{72}	Ga^{71}	8×10^{9}	Ge^{73}	4×10^{5}	As^{75}	7×10^{5}	9×10^{2}
	Zn^{69m}	Zn^{68}	3×10^{8}	Ga^{69}	$\sim10^{6}$	Ge^{72}	$\sim10^{5}$	------
XI.	Ca^{47}	Ca^{46}	7×10^{3}	Ti^{47}	3×10^{8}	Ti^{50}	1.2×10^{2}	------
	Sr^{87m}	Sr^{86}	7×10^{9}	------	------	Zr^{90}	5×10^{4}	------
XII.	Cs^{134}	Cs^{133}	1×10^{8}	Ba^{134}	1×10^{1}	------	------	------
	K^{42}	K^{41}	9×10^{7}	Ca^{42}	1.6×10^{4}	Sc^{45}	8×10^{5}	------
	Rb^{86}	Rb^{85}	6×10^{6}	Sr^{86}	2×10^{6}	Y^{89}	2×10^{1}	4×10^{0}

Analyses of the Bruderheim Chondrite

Introduction.

As a test of our analytical procedures, and to provide new information about the chemical homogeneity of a chondritic meteorite and the partitioning of elements among the major mineral phases, we have undertaken analyses of portions of the Bruderheim chondrite. This work is being done with Dr. Ursula Marvin of the Smithsonian Astrophysical Observatory, Cambridge, Massachusetts.

The Samples.

All samples were furnished to us by Dr. Marvin. The chips, free from fusion crust, ranging in size from 0.3 to 0.8 gm, were pulverized by us in a diamonite mortar, then weighed into quartz tubes and sealed for irradiation.

The phase separates were prepared by Dr. Marvin from material initially crushed and sieved by Dr. C. Merrihue. Separations were made using a magnetic separator, clerici solution, and by hand picking. Clerici solution was rinsed off with warm distilled water and methanol. All samples were found to be better than 95% pure, and probably better than 98% pure, by grain counting under the microscope and by x-ray diffraction. We used these samples as they were received, with no attempt at further purification.

Irradiations.

Whole-rock chips GS-8 and GS-9, and olivine separate GS-10 were irradiated for 2 hours at a flux of 1×10^{13} n/cm^2/sec. Later samples were irradiated for an initial period of a few hours, then allowed to cool, and irradiated a second time. This enhances the longer-lived activities (and matches the operating schedule of our reactor). Two sets of iron wire flux gradient monitors were used, one present for both irradiations, the other only for the second. A summary of the weights and irradiations is given in Table 13.

Results.

Preliminary results are presented, by group and by element, for the rock chips in Table 14 and for olivine, pyroxene, troilite, and metal in Table 15. Uncertainties accompanying individual values are standard deviations based on counting statistics. An average content

Table 13. Weights and conditions of irradiation for meteorite samples.*

	gm.	duration of irrad (hrs)	interim decay time(hrs)	duration of 2nd irrad (hrs)
GS 8	.3588	2.0	---	---
GS 9	.6694	2.0	---	---
GS 10	.4106	2.0	---	---
GS 11	.7094	2.0	112	2
GS 12	.7573	4.5	114	3.0
GS 13	.4286	7.6	111	3.5
GS 14	.4386	8.9	111	3.5
GS 15	.3296	8.0	112	3.8
GS 16	.4060	8.3	111	3.5
GS 17	---	---	---	---
GS 18	.4080	8.1	112	3.5
GS 19	.2578	9.0	114	3.5

* Neutron flux approximately 1 x 10^{13} n/cm^2/sec.

Table 14. Analytical Results for Individual Chips of the Bruderheim chondrite.

	GS-8	GS-9	GS-11	GS-12	GS-13	GS-14	Ave.	Error 1	Error 2	Data Used
Ag(ppm)	-----	-----	-----	.084±.036	-----	.14±.016				
Br(ppm)	9.9±.8	5.1±.3	1.2±.5	9.7± 1.6	1.5±.3	1.01±.02				
Au(ppb)	251± 5	257± 7	-----	210±.120	270± 100	235± 3	248	3	11	8,9,14
Pt(ppm)	.32±.15	-----	.43±.40	-----	.6±.6	.7±.7	.51	.25	.17	All
Ba(ppm)	4.7± 1.2	-----	6.2± 2.4	4.3±.5	6.6± 2.0	4.9±.7	5.3	.7	1.0	All
Ta(ppm)	.1±.1	-----	.077±.034	-----	-----	-----	.09	.05	.02	Both
Mn(%)	.281±.029	.318±.016	.298±.004	.321±.007	.274±.006	.35±.05	.298	.007	.021	Omit 14
In(ppb)	.4±.7	1.2±.4	4± 4	1.8± 1.8	1± 1	1.6± 1.6	1.2	.55	.55	Omit 11
As(ppm)	2.9± 0.9	4.0±.4	2.00±.10	1.91±.11	2.1±.8	4.05±.32	2.83	.22	.99	
Cu(ppm)	62± 42	-----	113± 21	118± 12	91± 9	92± 3	103.5	13	12	11-14
Pd(ppm)	.8±.8	.9±.9	.2±.2	.8±.5	1.9±.9	.5±.4	.85	.45	.57	All
Sb(ppm)	.09±.08	.04±.14	.08±.07	.22±.2	.38±.03	.14±.05	.182	.046	.124	Omit 9
Se(ppm)	-----	-----	-----	-----	10.4±.7	10.4± 2.7	10.4	1.4	0	Both
Fe(%)	-----	21.5± 5.4	30± 10	22.1± 5	23.1±.35	18.7± 1.4	21.4	1.9	1.7	9,12-14
La(ppm)	.87±.40	.47±.05	.77±.17	1.76±.07	1.23±.04	.41±.07	.93	.04	.48	Omit 8
Ce(ppm)	-----	1.7±.8	1.32±.24	4.7±.3	3.64±.02	1.10±.01	2.49	.18	1.6	Omit 8
Nd(ppm)	.3±.3	.83±.70	1.42±.36	.89±.33	1.11±.22	.65±.12	.98	.18	.30	Omit 8
Sm(ppm)	.68±.06	.240±.005	.443±.016	.242±.005	.135±.006	.189±.008	.250	.004	.12	Omit 8
Eu(ppm)	.29±.03	.105±.004	.133±.002	.082±.001	.063±.002	.084±.003	.093	.001	.027	Omit 8
Gd(ppm)	1.7± 1.3	.33±.14	.67±.53	.45±.04	.431±.034	.196±.064	.42	.11	.14	Omit 8
Tb(ppm)	.15±.09	.11±.05	.123±.011	.054±.033	.044±.004	.049±.004	.076	.012	.037	Omit 8

	GS-8	GS-9	GS-11	GS-12	GS-13	GS-14	Ave	Error 1	Error 2	Data Used
Dy(ppm)	.63±.07	.51±.10	.727±.053	.455±.010	.325±.019	.246±.008	.45	.02	.19	Omit 8
Ho(ppm)	.23±.21	.157±.022	.160±.077	.094±.005	.060±.003	.062±.004	.107	.016	.049	Omit 8
Er(ppm)	~.6	~.25±.2	.36±.27	.32±.07	.28±.06	.26±.06	.29	.07	.041	Omit 8
Yb(ppm)	.55±.28	.34±.04	.34±.06	.30±.04	.169±.004	.26±.01	.28	.02	.07	Omit 8
Lu(ppm)	-----	.048±.003	.035±.001	.049±.002	.031±.001	.040±.005	.041	.001	.008	Omit 8
Cr(%)	4,010± 980	3,760± 90	6040 ± 700	4350± 300	2250± 1100	-----	4080	330	1080	Omit 14
Hf(ppm)	.29±.23	.35±.15	.18±.16	1.03±.18	.44±.04	1.2±.4	.58	.09	.44	All
Sc(ppm)	8.2± 2.1	7.7± 1.3	8.0± 1.0	9.5±.6	7.8±.1	10.8±.8	8.7	.5	1.2	All
Ni(%)	1.34±.10	1.51±.12	1.30±.07	1.32±.08	1.37±.09	1.32±.04	1.33	.04	.03	Omit 9
Co(ppm)	422± 159	442± 29	432± 16	422± 31	427± 32	388± 21	422	28	18	All
Ga(ppm)	6± 5	5.2± 3.9	9.4± 4.3	9.1±.9	5.2± 2.5	9.3±.7				
Zn(ppm)	63± 12	44± 8	36± 5	45± 27	50± 6	65± 2	52	3	12	Omit 12
Ca										
Sr(ppm)	11± 4	18± 9	-----	12± 3	16± 3	10.1± 2.3	13	2.2	3.3	All
Cs(ppm)										
K										
Rb(ppm)										

Table 15. Analytical Results for Separated Phases of the Bruderheim Chondrite

	GS-15 Olivine	GS-18 Pyroxene	GS-16 Troilite	GS-19 Metal
Ag	-----	.05±.05	-----	.08±.01
Br				
Au	11.3± 1.3	-----	-----	3,150± 530
Pt	-----	-----	-----	6.3± 1.9
Ba	1.68±.23	2.7± 2.5	-----	.25±.19
Ta	-----	-----	-----	.26±.24
Mn	.128±.006	.251±.030	-----	.025±.007
In	.4±.1	10.6±.2	-----	-----
As	.3±.15	.15±.03	3.6± 1.8	36± 9
Cu	26.2± 6.7	49.3± 4.4	80± 11	718± 27
Pd	.006±.006	-----	.58±.28	3.8± 3.8
Sb		-----	.86±.14	1.8± 1.6
Se	-----	1.4±.6		.52±.04
Fe	16.5± 1.1	11.2±.2	64.0± 1.1	85.7± 1.4
La	1.15±.11		.048±.028	
Ce	2.15±.01		.14±.07	
Nd	.88±.10		.26±.26	
Sm	.255±.005		.0092±.003	
Eu	.026±.001		.004±.0006	
Gd	.30±.12		-----	
Tb	.035±.008		.008±.007	
Dy	.145±.020		.027±.001	
Ho				
Er	.22±.10		.025±.020	

	GS-15 Olivine	GS-18 Pyroxene	GS-16 Troilite	GS-19 Metal
Yb	.091±.012		.015±.010	
Lu	.017±.001		.0030±.0007	
Cr	498± 39	14.1±.4	7,760± 700	3030± 80
Hf	1.08±.07	2.7±.25	.37±.2	5.9±.6
Sc	4.2±.1	11.54±.05	.35±.09	1.24±.01
Ni	96±.20	.16±.02	.167±.007	13.4± 1.1
Co	-----	34.5±.5	146± 25	4710± 42
Ga	1.38±.38	.84±.05	21.1± 1.5	25.2± 2.5
Zn	73± 13	64± 3	9± 9	-----
Ca				
Sr	3.7± 1.3	16± 10	1.7± 1.2	-----
Cs	.06±.03		.002± .001	
K				
Rb	-----		.022±.011	

is presented for each element, and any individual values omitted from the average are indicated (usually, because of an uncertainty larger than for the other individual samples). Two sets of analytical uncertainties are given for these averages. The first is a measure of the analytical precision, and is the square root of the sum of the squares of the uncertainties of the individual analyses divided by the number of samples averaged. The second is a standard deviation based on the average and residuals for replicate analyses. Whenever the second error significantly exceeds the first, real inhomogeneity from chip to chip is being observed. When the first and second uncertainties are about the same size, any real variation is masked by analytical error. When the second is smaller than the first, it is fortuitous (as for Ta).

The analytical uncertainties in Table 15 are also based on counting statistics. The olivine results are mostly from sample GS-15, with GS-10, an earlier olivine analysis, used as a check on the later, more precise results.

Table 16 is an attempted mass balance for the meteorite, based at this point soley on the four major phases and the modal analysis of Duke et al. (1961). The accompanying errors are those propagated through the calculations from the errors listed in Tables 14 and 15, with no uncertainty in the modal analysis assumed.

Discussion.

The elements are discussed individually, then the metal phase, then limits on contamination of each phase by traces of the others. We emphasize that this is a progress report, not a final tabulation and comparison. The analytical results have not been finally screened for computational errors, nor thoroughly screened for minor interferences from other elements in the same counting group. These preliminary comparisons are made mostly with work summarized by Mason (1962) plus a few more recent, handy reports. Whenever a reference included in Mason's book is used, and "M" follows the date, and the reference is not included in our bibliography whether we consulted it or not.

Ag. This element was not sought until after Sample GS-11 was analyzed, when its gamma lines first appeared with significant intensity in a late count. The data are incomplete. The whole rock level is in

Table 16. Mass balances for the Bruderheim chondrite.

	Adjusted Mode	Fe %	Ni %	Co ppm	Cu ppm	Au ppb	Pt ppm
Olivine	.411	6.78±.45	.0004±	-----	10.8± 2.8	4.6±.53	-----
Pyroxene	.428	4.80±.09	.0685±	14.8±.2	21.1± 1.9	-----	-----
Troilite	.068	4.35±.08	.0113±.005	9.9± 1.7	5.4±.8	-----	-----
Metal	.077	6.60±.11	1.03±.085	362.7± 3.2	55.3± 2.1	242.6± 41	.49±.15
Sum	1.001	22.53±.48	1.11±.09	387.4± 13	92.6±6.7	247± 41	.49±.15
/whole rock	----	1.05±.09	.834±.070	.92±.07	.89±.14	1.00±.17	.96±.55

	Ta ppm	Ag ppm	As ppm	Sb ppm	Pd ppm	In ppb	Ga ppm
Olivine	-----		.12±.06	-----	.0025±.0025	.16±.04	.57±.16
Pyroxene	-----		.06±.01	-----	-----		.36±.02
Troilite	-----		.24±.12	.058±.010	.039±.019		1.43±.10
Metal	.020±.018		2.77±.69	.139±.123	.29±.29		1.94±.19
Sum	.020±.018		3.2±.70	.20±.12	.33±.29		4.30±.27
/whole rock	.22±.2%		1.13±.48	1.1± 1.0	.39±.43		.58±.17

	Sc ppm	Zn ppm	Ba ppm	Mn %	Sr ppm	Cr
Olivine	1.73±.04	30± 5	.69±.09	.053±.002	1.52±.33	205± 16
Pyroxene	4.94±.02	27± 1	1.16± 1.07	.107±.013	6.85± 4.3	6± 0
Troilite	.02±.01	.6±.6	-----	-----	.12±.08	528± 48
Metal	.10±.00	-----	.02±.01	.002±	-----	233± 6
Sum	6.78±.05	58± 5.1	1.86± 1.07	.162±.013	8.5± 4.3	972± 51
/whole rock	.78±.06	1.12±.28	.35±.21	.54±.06	.65±.37	.24±.06

line with the results of Shindewolf and Wahlgren (1960M)(ave. .094ppm). The metal phase does not contain enough Ag to account for its whole rock abundance, and no value is yet available for the troilite.

Br. There is much scatter among the whole-rock analyses for Br, and the level is an order of magnitude too high, compared with the values of Reed and Allen (1966). The separated phases contain more Br than needed for a mass balance. We conclude that, despite not using halogen containing liquids in the mineral separations, all the samples are contaminated with Br. The separations were done in a laboratory in which bromoform was being used.

Cl. The interference from K is so great that only samples for which the ratio of K to Cl is less than 10 can be done in our reactor.

Au. This element can be detected at the ppb level, and good precision (2-5%) can be obtained at the hundred ppb level. Our average value of 248 ppb for the whole rock is in line with values given by Vincent and Crocket (1960M). The concentration of Au in the pyroxene was below our detection limit, while a surprising 11 ppb were detected in the olivine. This latter value cannot be due to metal in the olivine, since the content of Ni sets too low a limit for contamination by that phase. No value is yet available for the troilite, but the element is so concentrated in the metal phase that a good mass balance was obtained.

Ba. At the ppm level the precision is in the range 10-15%. The average of 5.3 ppm is a little above the results of Reed et al. (1960M). for other chondrites, but overlaps the value of $4.3 \pm .3$ ppm given by Shima and Honda (1967). Chip-to-chip variation does not significantly exceed the analytical precision. A surprisingly high amount was found in the metal phase, as is true also for Sc and the REE. The reason is not clear, since the amount of pyroxene contaminant necessary to account for it considerably exceeds the amount believed to be present. The mass balance shows that only 35% of the Ba has been accounted for. Possibly the rest of that element is concentrated in the feldspar.

Pt. The precision for this element is very poor, but the level of 0.5 ppm is established, good to perhaps $\pm$ 50%. Baedecker and Ehmann (1965) give 0.9 ppm. Of the mineral separates, the metal

phase contained a measurable amount. The mass balance is quite satisfactory, considering the precision.

Ta. This is another borderline element, and the level of .09 ppm is about 3 times higher than found for other chondrites (Atkins and Smales, 1960M). The mass balance is poor. We draw no conclusions about the phase partition of Ta.

Mn. The precision for this element is excellent. It activates so well and is sufficiently abundant that it must be carefully removed from other element groups before their radioassay. The 0.298% Mn we found exceeds the average of .240% of Wiik (1956M) and .26% of Moore and Brown (1962M), but is only slightly above the value of .280 $\pm$ .05% given for Bruderheim by Schmitt and Smith (1963). The variation from chip to chip exceeds the precision, and amounts to a few percent. The mass balance shows only half of the Mn to be accounted for, but there is no value for the sulfide phase, which could contain the needed amount.

In. Although this element is easily measured in terrestrial rocks, the precision is poor here owing to the extremely low concentration and the inability to resolve the principal gamma peaks from those of Fe. The level of 1 ppb established for the whole rock is in line with results of Schindewolf and Wahlgren (1960M). No value is yet available for the troilite.

As. The precision for this element is 10% or better, but the abundance varies from chip to chip by a factor of 2. The average of 2.8 ppm is in good agreement with the results of Onishi and Sandell (1955M). Those investigators also examined separated phases from composites of chondrites and found 12, 10, and 0.3 ppm in the metal, sulfide, and silicate. We found ten times more in the metal as in the sulfide phase. The mass balance is quite satisfactory, but subject to the large uncertainty for the whole rock.

Cu. The precision for Cu is about 10%, and the variability from chip to chip is not appreciably, if any, greater. The average of 104 ppm agrees well with the range found by Wiik (unpublished, M) and by Smales et al. (1957, 1958 M). The element appears in all the major meteorite phases, and the mass balance is satisfactory, although low and just outside one standard deviation uncertainty.

Pd. This is another borderline element, but the level of 0.8 ppm for the whole rock is in reasonable agreement with the value 1.0 given by Greenland (1967). The mass balance is unsatisfactory. We are not confident of our analysis for this element.

Sb. Longer irradiations have improved the precision for Sb to the 8-30% range. The average value of 0.18 ppm is reasonable when compared with the average of 0.1 ppm found by Onishi and Sandell (1955bM) for composites of chondrites. Sb contents appear to vary well outside the analytical uncertainty as did As values, but not in the same samples. The mass balance is satisfactory, but not too informative because of poor variations in the whole rock Sb contents. Both the metal and troilite phases are important carriers of Sb, unlike the result for As and unlike the results of Onishi and Sandell in which the Sb is predominantly in the metal phase.

Se. This element was not sought until its gamma lines appeared with adequate intensity in GS-12. The precision is a few percent when the chemical yield is good. The average value of 10.4 ppm for the whole rock is in the range found by DuFresne (1960M) and by Schindewolf (1960M). Unfortunately, the troilite value was lost due to poor chemical yield and an error in the standard, but the low Se concentrations in the other phases support the expectation that most of that element is in the sulfide phase.

Fe. Wet chemical neutron activation analysis for Fe as a major element is perhaps a little unusual, but since the element must be extracted to keep it from interfering with precipitates of the sulfide group, it would be wasteful not to measure it. The Fe value of 21.4 $\pm$ 1.9% for the whole rock agrees within the uncertainty with 22.28 to 23.11% found by Nichiporuk et al. (1967). Pure FeS would contain 63.5% Fe; we found 64 $\pm$ 1% in the troilite. Olivine (Fe_{22}) (Duke et al., 1961) would contain 15.9% Fe; we found 16.5 $\pm$ 1.1%. Pyroxene (Fs_{22}) would contain 11.5% Fe; we found 11.2 $\pm$ .2%. Also, the mass balance for the metal phase is excellent, and the mass balance for Fe in the meteorite is satisfactory.

REE. The precision for the individual REE is discussed in section 1 of the report. The actual precision for these analyses is somewhat poorer due to low chemical yields, a problem which has now been corrected.

It was surprising to discover the variability of these elements, both in absolute concentration and in relative abundance distribution, from chip to chip. No comparison diagram is presented because the data are not yet final. The abundances in GS-8 are 2-3 times higher than the average for chondrites (Schmitt and coworkers in Haskin et al., 1966 and Haskin et al., 1968), with Eu and Sm up to 4 times the average. In GS-9, all elements are about 1.5 times the chondrite average. In GS-11, all are 2-3 times the chondrite average except Yb (1.7 times) and Lu (1.0 times). In GS-12, La and Ce are more than 5 times the average, Sm and Eu 1.2 to 1.3 times, and the other elements about 1.5 times. In GS-13, La and Ce are about 4 times the average, the rest about 0.9 times except Sm, only 0.75 times. In GS-14, the light and heavy REE are concentrated 1.2 to 1.3 times the average, but the elements Sm through Ho are only about equal to the average. The average of all chips except GS-8 (omitted because of its very large analytical uncertainties) is about 1.5 times the average concentration for the elements Nd-Lu, and 3 times the average for La and Ce. Inclusion of GS-8 would raise the values uniformly by a few percent. Some variability both in relative and absolute abundances has been observed before, but not to this extent. The average concentrations for Bruderheim exceed those found for other chondrites. They are only a little higher than the values reported for a separate sample by Shima and Honda (1967).

Data for separated phases are too incomplete to attempt a mass balance. Comparison of our olivine and troilite values with the measurements of Shima and Honda is not feasible, because their sample contained the phosphates in addition to a mixture of those phases. It is to be expected that phosphates and feldspar phases must be analyzed before a good mass balance can be made. The olivine phase shows preferential incorporation of the light REE and a deficiency of Eu, relative to the whole rock. These relative abundance trends are in line with those observed in terrestrial rocks for olivine in contact with pyroxene and feldspar. The olivine has higher absolute RE contents than most terrestrial olivines, and is an important host for REE in the meteorite. This may be because the amounts of Ca containing clinopyroxene and phosphate phases, which tend to concentrate the REE more than do olivine or hypersthene, are in such low abundance.

in the meteorite. The missing Eu is presumably in the feldspar, as would be expected and as is indicated by the data of Shima and Honda.

Cr. The precision for Cr is a few percent for longer irradiations. The average of 4080 ppm is lower than the 4550 ± 90 found by Schmitt and Smith (1963) and well above the range of 2400 to 2700 ppm found by Nichiporuk et al. (1967), but the individual values cover this entire range. Such variability in Cr content is nothing new (Urey and Craig, 1953M; Wiik, 1956M). Most of the Cr is in chromite (Duke et al., 1961), which accounts for the apparently poor mass balance. Inhomogeneous distribution of chromite could also explain the chip to chip variation in Cr content.

Hf. The precision for this element is very poor. The crude average of 0.6 ppm is in the range reported by Merz (1962M). The data for the mineral separates are too poor to present.

Sc. The precision for Sc is about 2%. The average of 8.7 ppm is in line with the observations of Bate et al. (1960M), Kemp and Smales (1960M) and of 8.4 ± .8 ppm reported for Bruderheim by Schmitt and Smith (1963). The variability from chip to chip is about 3 times the analytical uncertainty, so is presumably real. For unknown reasons, the Sc contents of the minerals fall about 20% short of giving a good mass balance. The phosphate phases may contain the missing Sc. The 1.2 ppm for the metal phase is not reasonable, but matches the equally unreasonable Ba content.

Ni. The precision for Ni is now a few percent at the whole-rock level of 1.33%. The quantity of Ni in the various chips is quite constant, testifying to a uniform metal phase content of the chips. The pyroxene contains nearly as much Ni as the troilite. Most of the Ni is in the metal phase. The mass balance is a few percent short.

Co. The precision for Co is now 5% at the whole-rock level of 422 ppm. This value agrees very well with that of 440 ± 20 found by Schmitt et al. (1963). Most of the Co is in the metal phase, and the variation from chip to chip is thus low. The 146 ppm found in the troilite are well under the 547 ppm obtained for troilite from another chondrite by Nichiporuk and Chodos (1959M). The mass balance is on the low side, but satisfactory.

Ga. The precision for Ga is now apparently in the 8-10% range. The level of 7.4 ± 2.1 ppm overlaps the upper edge of the range given by Onishi and Sandell (1956M). The concentrations in the metal and troilite are about equal, in line with the results of Onishi and Sandell. Less than 60% of the Ga is accounted for in the analyzed phases. Some of the remainder may be in the feldspar. Alternatively, our average value for the whole rock may be too high.

Zn. The precision for Zn is in the range 4-10%. The level of 52 ppm agrees well with the average of 50 ppm given by Nishimura and Sandell (1962M). Their results for silicate and troilite phases are also similar to ours. The mass balance is satisfactory.

Sr. The precision is about 20% for Sr. The value of 13 ppm is within the range found by Pinson et al. (1953M). The variability from chip to chip is a little greater than the precision; whether this is real is not certain. The mass balance is adequate, owing to large analytical uncertainties, but the value is low enough to accommodate a significant Sr contribution from feldspar.

Ca, Alkali metals. The data for these elements have not yet been processed.

The metal phase. This is the only phase for which all the major constituents were analyzed. The sum of the abundances of Fe, Ni, Co, Cr, Mn, and Cu accounts for 99.97% of the metal phase. This remarkably excellent mass balance has, however, an uncertainty of 1.8%, so that the last digit is not significant. An upper limit of about 2-3% silicate in the metal phase is set by these results. This makes the relatively high amounts of Sc and Ba (and the REE, based on very preliminary data), corresponding to about 10% contamination of the metal phase by pyroxene alone, very puzzling.

Cross contamination among phases.

A high concentration for an element in one of the phases can be used to set an upper limit for the presence of that phase in another phase in which the concentration of the element is low. For example, the Ni content of the metal phase is 134,000 ppm, but in the olivine separate is only 96 ppm. Contamination of the olivine with metal phase cannot therefore exceed 96/134,000, or 0.07% by

weight. A low amount of metal contamination in the olivine sample is confirmed by the data for Co, Au, Ga, and Pd, which give upper limits ranging from 0.1 to 0.6%.

Upper limits for metal phase in the pyroxene sample are obtained from Co, Au, Ga, and Cr, and range from 0.16 to 0.7%. For metal contamination of the troilite, an upper limit of 1.2 to 3% is set by Co and Ni.

Troilite contamination of the metal phase is set at less than 0.3%, assuming a sensitivity of 0.1 ppb for In. Troilite in the pyroxene does not exceed 0.2% according to the Cr data. Results for In place an upper limit of 1% for troilite in olivine. A firm Se value for the troilite will probably reduce these limits further.

Few of the elements examines so far are sufficiently higher in the silicate than in the troilite and metal phases or different enough between silicate phases that useful upper limits for contamination can be set in this fashion. The amount of pyroxene in olivine, for example, is only limited by the Ni values to 6%, but grain counting shows much less to be present. Sc values limit pyroxene contamination in the troilite to 3%. Upper limits of only 10% pyroxene contamination in the metal can be set from the Mn and Sc data, but the amount of silicate is limited by the mass balance for the metal phase to 2-3%.

Contamination of pyroxene by olivine cannot exceed 3%, according to Cr data. La values limit the olivine contamination of troilite to below 5%. Olivine in the metal phase is limited to 15% by Ba concentrations, again a value well above the limit set by the mass balance for the metal phase and by grain counting. Data for the alkali metals should reduce the limits obtained by this method for contamination by the silicate phases.

The work in this section was done by R. O. Allen, L. A. Haskin, M. A. Anderson, J. W. Blackbourn, and K. A. Zweifel.

Bibliography

Note: All references ending in M are found in Mason (1962).

Baedecker, P.A. and Ehmann, W.D. (1965) The distribution of some noble metals in meteorites and natural materials. Geochim. Cosmochim. Acta 29, 329-342.

Cobb, J.C. (1967) Determination of lanthanide distribution in rocks by neutron activation and direct gamma counting. Anal. Chem. 39, 127-131.

Denechaud, E.B. (1969) Rare-earth activation analysis: improvement and application to Stretishorn dike and Duluth complex. Ph.D. thesis, Univ. of Wisconsin.

Duke, M., Maynes, D., and Brown, H. (1961) The petrography and chemical composition of the Bruderheim meteorite. J. Geophys. Res. 66, 3557-3563.

Frey, F.A. (1969) Rare-earth abundances in a high-temperature peridotite intrusion. Submitted for publication.

Frey, F.A., Haskin, M.A., Poetz, J.A., and Haskin, L.A. (1968) Rare-earth abundances in some basic rocks. J. Geophys. Res. 73, 6085-6098.

Gunn, B.M. and Watkins, N.D. (1969) The petrochemical effect of the simultaneous cooling of adjoining basaltic and rhyolitic magmas. Geochim. Cosmochim. Acta 33, 341-356.

Haskin, L.A. and Frey, F.A. (1966) Dispersed and not-so-rare earths. Science 152, 299-314.

Haskin, L.A., Frey, F.A., Schmitt, R.A. and Smith, R.A. (1966) Meteoritic, solar, and terrestrial rare-earth distributions. Phys. Chem. Earth, vol. 7, 167-321.

Haskin, L.A., Haskin, M.A., Frey, F.A., and Wildeman, T.R. (1968) Relative and absolute terrestrial abundances of the rare earths, pp 889-912 in Origin and Distribution of the Elements, L.H. Ahrens, ed., Pergamon, Oxford.

Haskin, L.A., Wildeman, T.R., and Haskin, M.A. (1968) An accurate procedure for the determination of the rare earths by neutron activation. J. Radioanal. Chem. 1, 337-348.

Lukens, H.R., Jr. (1964) Estimated photopeak specific activities in reactor irradiations. Gulf General Atomic report GA-5073 (Excerpt).

Mason, B. (1962) Meteorites, Wiley, New York.

McIntire, W.L. (1963) Trace element partition coefficients--a review of theory and applications to geology. Geochim. Cosmochim. Acta 27, 1209-1264.

Nichiporuk, W., Chodos, A., Helin, E., and Brown, H. (1967) Determination of iron, nickel, cobalt, calcium, chromium, and manganese in stony meteorites by x-ray fluorescence. Geochim. Cosmochim. Acta 31, 1911-1930.

Onuma, N., Higuchi, H., Wakita, H., and Nagasawa, H. (1968) Trace element partition between two pyroxenes and the host lava. Earth Planet Sci. Letters 5, 47-51.

Philpotts, J.A. and Schnetzler, C.C. (1968) Europium anomalies and the genesis of basalt. Chem. Geol. 3, 5-13.

Philpotts, J.A., and Schnetzler, C.C. (1968) Genesis of continental diabases and oceanic tholeiites considered in light of rare-earth and barium abundances and partition coefficients. p940, in Origin and Distribution of the Elements, L.H. Ahrens, ed, Pergamon, Oxford.

Reed, G.W. and Allen, R.O. (1966) Halogens in chondrites. Geochim. Cosmochim. Acta 30, 779-800.

Schilling, J.G. and Winchester, J.W. (1966) Rare earths in Hawaiian basalts. Science, 153, 867-869.

Schmitt, R.A. and Smith, R.H. (1963) Abundances of Na, Sc, Cr, Mn, Fe, Co, and Cu in 92 meteorites, 9 terrestrial specimens, and 90 individual chondrules. General Atomic report GA-4782.

Schnetzler, C.C. and Philpotts, J.A. (1968) Partition coefficients of rare-earth elements and barium between igneous matrix material and rock-forming-mineral phenocrysts. pp 929-939 in Origin and Distribution of the Elements, L.H. Ahrens, ed, Pergamon, Oxford.

Shima, M. and Honda, M. (1967) Distributions of alkali, alkaline earth, and rare-earth elements in component minerals of chondrites. Geochim. Cosmochim. Acta 31, 1995-2006.

Tomura, K., Higuchi, H., Miyaji, N., Onuma, N., and Hamaguchi, H. (1968) Determination of rare-earth elements in rock samples by neutron activation analysis with a lithium-drifted germanium detector after chemical group separation. Anal. Chim. Acta. 217-228.

REPORT DISTRIBUTION LIST FOR CONTRACT NO* NAS-9-7975

Dr. E. Anders
Enrico Fermi Institute for Nuclear Studies
University of Chicago
Chicago, Illinois

Dr. Robert A. Arnott
Chemistry Department
Wisconsin State University
Oshkosh, Wisconsin 54901

Dr. Douglas G. Brookins
Department of Geology and Geography
Kansas State University
Manhattan, Kansas 66502

Dr. Kent C. Condie
Department of Earth Sciences
Washington University
St. Louis, Missouri 63130

Dr. W. D. Ehmann
Department of Chemistry
University of Kentucky
Lexington, Kentucky

Dr. Fred A. Frey
Department of Geology
Massachusetts Institute of Technology
Cambridge, Massachusetts 02139

Dr. Paul W. Gast
Lamont Geological Observatory
Columbia University
Palisades, New York 10964

Dr. Gordon Goles
Department of Geology
University of Oregon
Eugene, Oregon 97403

Dr. Bernard M. Gunn
Department of Geology
Universite de Montreal
Case postale 6128, Montreal 3

Dr. B. H. Mason
Division of Meteorites
U.S. National Museum
Washington, D.C. 20560

Dr. John A. Philpotts
Laboratory for Theoretical Studies
Goddard Space Flight Center
Greenbelt, Maryland 20771

Dr. George W. Reed,Jr.
Chemistry Division
Argonne National Laboratory
9700 So. Cass Avenue
Argonne, Illinois 60440

Dr. Keith A. Richardson/TH
NASA Manned Spacecraft Center
Lunar and Earth Sciences Division
Houston, Texas 77058

Dr. Jean-Guy Schilling
Narragansett Marine Laboratory
University of Rhode Island
Kingston, Rhode Island 02881

Mr. L. T. Schmiech/BG921
NASA Manned Spacecraft Center
Space Sciences Procurement Branch
Houston, Texas 77058

Dr. R. A. Schmitt
Department of Chemistry
Oregon State University
Corvallis, Oregon 97331

Dr. Karl K. Turekian
Department of Geology
Yale University
New Haven, Connecticut 06520

Dr. G. J. Wasserburg
Department of Geophysics
California Institute of Technology
Pasadena, California

Dr. Norman Watkins
Department of Geology
The Florida State University
Tallahassee, Florida 32306

T. R. Wildeman
Chemistry Department
Colorado School of Mines
Golden, Colorado 80401